# Chapter 4

# O VI Absorption in the Milky Way

## 4.1 Introduction

Highly ionized gas spanning the temperature range from $10^5$ to $10^7$ is an important constituent of the Interstellar medium (ISM) of galaxies. In the UV range, highly ionized species for e.g. Si IV, C IV, N V and O VI show strong transitions signifying the presence of tenuous gas through their absorption features. Among these ions, the $O^{+5}$ (O VI) ion absorption doublets at 1032 Å and 1038 Å stands out as an important tool to help understand various physical processes of the ISM of galaxies. O VI is unlikely to arise from photoioization as 113.9 eV is required to remove one more electron from O V, rather it is produced in the ISM through collisional ionization at temperatures of around $3\times10^5$ K [298, 299]. Such temperatures represent the interface of warm ($T \sim 10^4$ K) and hot ($T > 10^6$ K) interstellar gas. Thus the interstellar O VI absorption and emission may be used as a sensitive scale to study the interface matter, its structure and distribution. The detailed analysis of O VI absorption helps in understanding the kinematics and velocity distribution associated with the gas, the total abundance and its comparison with other species and the processes leading to its formation in the ISM [300].

In the 1990's the *Copernicus* satellite [301, 302] and the *Hopkins Ultraviolet Telescope (HUT)* [303] were the main instruments used for studying the O VI absorption with a limited spectral resolution. The launch of the *Far Ultraviolet Spectroscopic Explorer (FUSE)* [304, 305] in 1999 June has resulted in the study

of O VI with much higher resolution and high signal to noise. The *FUSE* has a far-ultraviolet wavelength coverage of 905 – 1187 Å and a resolution of $\sim$ 15,000–20,000 near O VI line absorption wavelength, that fits very well for a detailed study of the O VI lines in the nearby universe. The study of O VI absorption in the ISM of galaxies with the *FUSE* has given us information about the formation and distribution of O VI in the Milky Way and the Magellanic Clouds that adds to our knowledge of varying ISM conditions in environments of different metallicities [306–312]. Apart from absorption studies, the *FUSE* has also been used to observe the O VI spectra in emission from the diffuse ISM in the MW [313–315] and superbubbles (SBs) in the LMC [316]. The O VI absorption studies at low redshifts trace the warm-hot intergalactic medium (WHIM) and is an important contributor to model the cosmological problem of missing baryons [317].

## 4.2 O VI in the Milky Way

The study of the physical characteristics and the distribution of hot interstellar gas of the Milky Way started with launch of *Copernicus* satellite that probed O VI absorption towards several relatively nearby stars in the local interstellar medium [301, 318]. However, the range of possible studies on O VI absorption has been enhanced in a great way after the lunch of *FUSE*. Strong O VI absorption in the Galactic halo was detected along 10 out of 11 lines of sight in the range log N(O VI) from 13.80 to 14.64 atoms cm$^{-2}$ by Savage et al [307]. O VI absorption in the halo of the Milky Way was studied by Howk et al. [306] and they found the mean column density of O VI to be $14.52^{+0.10}_{-0.14}$ atoms cm$^{-2}$ towards the LMC. This study also reports the existence of a widespread but irregular distribution of O VI in the MW halo. Properties of O VI in the Galactic halo have been studied by Savage et al. [343] using *FUSE* observations of 100 extragalactic sight lines. They found the average log N(O VI) value as 14.36 atoms cm$^{-2}$, while log N(O VI) sin |b| for the complete sample to be 14.21 atoms cm$^{-2}$. Oegerle et al. [309] have reported a survey of O VI absorption in the ISM towards 25 white dwarfs. They report O VI detections with $\geq$2 $\sigma$ significance toward 14 of the 25 stars with average O VI column densities $2.4\times10^{8}$ cm$^{-2}$. Bowen et al. [319] studied absorption lines

of O VI toward 148 early-type stars situated at distances $\geq$1 kpc and found an average O VI midplane density $1.3\times10^{-8}$cm$^{-3}$. Savage & Lehner [310] detected O VI absorption with $\geq2$ $\sigma$ significance in the local interstellar medium (LISM) along 24 of 39 lines of sight. They found column densities in the range log N(O VI) = 12.38 to 13.60 atoms cm$^{-2}$.

A survey of O VI absorption in the LMC was done by Pathak et al. [312] in which they used the *FUSE* observational data of 70 lines of sight. Towards all the lines of sight, these observations also have a MW component that remains to be studied. In this work the *FUSE* observations of interstellar O VI in the MW as observed towards 70 lines of sight along the LMC has been studied.

## 4.3 Observations and Data Reduction

Description about the *FUSE* instruments is given by Moos et al. [304] and Sahnow et al. [305], a brief description is given here. *FUSE* consists of two channels (SiC and LiF) optimized for both short and long wavelengths. These channels are further divided into eight different segments; the SiC 1A, SiC 2A, SiC 1B, SiC 2B segments covering the wavelength range 905 – 1105 Å and LiF 1A, LiF 2A, LiF 1B and LiF 2B segments covering the wavelength 1000 - 1187 Å. *FUSE* observes through three apertures- LWRS, MDRS and HIRS with aperture size 30×30, 4×20 and 1.25×20 arcsec$^2$ respectively. Here LiF 1A data has been used as the sensitivity of this near 1032 Å is almost double to that of other segments. Here data acquired with the LWRS and the MDRS apertures are only considered. [305].

The fully calibrated *FUSE* spectra are available for download from the Multimission Archive at STScI (MAST). These are processed by the latest *FUSE* data reduction pipeline CALFUSE version 3.2 [180]. Though, the *FUSE* has more than 600 observations in and around the LMC, here we report analysis of 70 lines of sight. Detail log for these lines of sight is presented in Table 4.1. These 70 *FUSE* lines of sight are selected because of the simplicity of the continuum fitting in the vicinity of O VI. Out of these 70 sight lines, Friedman et al. [321] studied O VI absorption for 1 line of sight, 11 of these have been reported by Howk et al. [320]

survey, 3 sight lines by Danforth et al. [322] and 1 sight line by Lehner and Howk [323]. Danforth et al. [324] prepared an atlas of *FUSE* observations in the Magellanic Clouds where 57 LMC stars and 37 Small Magellanic Cloud (SMC) were included. Blair et al. [325] have extended this to produce a more extensive atlas that includes *FUSE* observations towards 287 stars from the Magellanic clouds and has been referred for spectral type of background stars and other information. *FUSE* offers a reasonably good resolution of 20 km $s^{-1}$. All the spectra reported here are downgraded to 35 km $s^{-1}$ to have a higher signal-to-noise. This has been done for all the spectra irrespective of the quality to maintain uniformity.

### 4.3.1 Continuum and Contamination

Defining a stellar continuum level near the O VI profile is the first step for analyzing the absorption profile. Following the method described in Sembach & Savage [342] and Howk et al. [320] all continuum are fitted with Legendre polynomial. The shape of the local stellar continuum near the interstellar O VI 1031.926 Å absorption for each stars are estimated by fitting Legendre polynomial. Though a low order polynomial ($\leq$5) is simply enough to model the continuum, there are few lines of sight which show complex behaviour near O VI absorption (for e.g., Sk-67D05, Sk-67D168, Sk-70D115 etc.) as shown in Figure 4.1.

The complexity in the continuum fitting for these sight lines arises as a result of sudden local dip or a sharp rise near the O VI absorption. It is found that, for these lines of sight, a comparatively higher order polynomial is required in fitting the continuum. Several continua have been tested and in the O VI column density measurement the uncertainties involved were used. It should be noted that correction for any stellar wind absorption features are not done. The normalized spectra for all 70 lines of sight in a region that is near to the O VI absorption at 1032 Å have been presented in Figure 4.2.

**Table 4.1:** *FUSE* observation log for all considered (70) sight lines.

| *FUSE* ID | Object Name | *FUSE* Aperture | RA | Dec | Spectral Type | V mag. | Reference |
|---|---|---|---|---|---|---|---|
| P1030703 | SK-67D05 | LWRS | 04 50 18.96 | -67 39 37.9 | O9.7Ib | 11.34 | [326] |
| A0490402 | SK-68.03 | LWRS | 04 52 15.56 | -68 24 26.9 | O9I | 13.13 | [327] |
| E5111901 | BI13 | LWRS | 04 53 06.48 | -68 03 23.1 | O6.5V | 13.75 | [328] |
| D0980801 | SK-67D18 | MDRS | 04 55 14.90 | -67 11 24.5 | O6-7n-nm+WN5-6A | 11.95 | [326] |
| P1174401 | Sk-67D20 | LWRS | 04 55 31.50 | -67 30 01.0 | WN4b | 13.86 | [329] |
| B0100201 | PGMW-3070 | MDRS | 04 56 43.25 | -66 25 02.0 | O6V | 12.75 | [325] |
| D0300302 | LH103102 | MDRS | 04 56 45.40 | -66 24 45.9 | O7Vz | 13.55 | [325] |
| D0300101 | LH91486 | MDRS | 04 56 55.58 | -66 28 58.0 | O6.5Vz | 14.2 | [325] |
| B0100701 | PGMW-3223 | MDRS | 04 57 00.80 | -66 24 25.3 | O8.5IV | 12.95 | [325] |
| F9270604 | HV2241 | LWRS | 04 57 15.83 | -66 33 54.8 | O7-III | 13.5 | [325] |
| P1174901 | HD32402 | LWRS | 04 57 24.19 | -68 23 57.2 | WC | | [328] |
| Z9050801 | SK-67_32 | LWRS | 04 59 52.30 | -67 56 55.0 | WN | 14.48 | [328] |
| P1030901 | SK-65D21 | LWRS | 05 01 22.33 | -65 41 48.1 | O9.7Iab | 12.02 | [330] |
| B0770201 | HV2274 | LWRS | 05 02 40.96 | -68 24 21.3 | B0-B2III-I | 14.2 | [325] |
| P1174501 | Sk-66D51 | LWRS | 05 03 10.20 | -66 40 54.0 | WN8h | 12.71 | [329] |
| D1380201 | NGC1818-D1 | LWRS | 05 04 32.56 | -66 24 51.0 | B0-B2V-IV | 14.93 | [325] |
| P1172101 | SK-70D69 | LWRS | 05 05 18.73 | -70 25 49.8 | O5V | 13.94 | [330] |
| P1171703 | Sk-67D69 | LWRS | 05 14 20.16 | -67 08 03.5 | O4III(f) | 13.09 | [331] |
| C1030101 | MACHO78-6097 | LWRS | 05 18 04.70 | -69 48 19.0 | B0-B2V-IV | 14.4 | [325] |
| E5112902 | BI130 | LWRS | 05 18 06.06 | -69 14 34.5 | O8.5V((f)) | 12.53 | [328] |
| Z9050201 | SK-69_94 | LWRS | 05 18 14.53 | -69 15 01.0 | B0-B2III-I | 9.72 | [325] |
| D9044701 | SNR0519-697 | LWRS | 05 18 44.20 | -69 39 12.4 | Supernova-remnant | | |
| D0880104 | BREY22 | MDRS | 05 19 16.40 | -69 39 19.5 | WC/O9.5Ib | 12.3 | [326] |
| B0270101 | HD269445 | LWRS | 05 22 59.87 | -68 01 46.6 | WN | 11.45 | [326] |
| P1173602 | SK-69D124 | LWRS | 05 25 18.37 | -69 03 11.1 | O9Ib | 12.81 | [327] |
| D1530104 | SK-67D105 | LWRS | 05 26 06.37 | -67 10 57.6 | Of | 12.42 | [325] |
| A1110101 | SK-67.106 | MDRS | 05 26 15.20 | -67 29 58.3 | B0-B2III-I | 11.78 | [332] |
| A1110201 | SK-67.107 | MDRS | 05 26 20.67 | -67 29 55.4 | B0-B2III-I | 12.5 | [332] |
| C1510101 | HD36521 | LWRS | 05 26 30.32 | -68 50 25.4 | WC | 12.42 | [333] |
| P1031402 | SK-68D80 | LWRS | 05 26 30.43 | -68 50 26.6 | WC4+OB | 12.40 | [334] |
| P2030104 | SK-68D82 | LWRS | 05 26 45.31 | -68 49 52.8 | WN5?b+(B3I) | 9.86 | [325] |
| P1173701 | BI170 | LWRS | 05 26 47.79 | -69 06 11.7 | O9.5Ib | 13.09 | [335] |
| C1550201 | SK-67D111 | LWRS | 05 26 47.95 | -67 29 29.9 | O6:Iafpe | 12.57 | [335] |
| F9270701 | HV2543 | LWRS | 05 27 27.40 | -67 11 55.4 | O8+O9 | 12.92 | [325] |
| P1172501 | SK-70D91 | LWRS | 05 27 33.74 | -70 36 48.3 | O6.5V | 12.78 | [335] |
| P1172303 | Sk-66D100 | LWRS | 05 27 45.59 | -66 55 15.0 | O6II(f) | 13.26 | [330] |
| E9570301 | HDE269599 | LWRS | 05 28 22.68 | -69 08 32.2 | Be | 10.18 | [325] |
| M1142001 | SK-65.63 | LWRS | 05 28 39.50 | -65 39 01.1 | O9.7I | 12.56 | [336] |
| C1030201 | HV982 | LWRS | 05 29 52.50 | -69 09 22.0 | B0-B2V-IV | 14.6 | [325] |
| E5113602 | SK-70D97 | LWRS | 05 30 11.35 | -70 51 42.2 | O9III | 13.33 | [325] |
| P1175001 | Sk-67D144 | LWRS | 05 30 12.22 | -67 26 08.4 | WC4+OB | 13.6 | [337] |
| P2170301 | BI184 | LWRS | 05 30 30.60 | -71 02 31.3 | B0-B2V-IV | 13.84 | [328] |
| D1380301 | NGC2004-B15 | MDRS | 05 30 36.58 | -67 17 42.3 | B0-B2V-IV | 14.18 | [325] |
| Z9050601 | SK-71_38 | LWRS | 05 30 38.77 | -71 01 47.9 | WC | 13.1 | [325] |
| P1031502 | Sk-71D45 | LWRS | 05 31 15.55 | -71 04 08.9 | O4-5III(f) | 11.51 | [326] |

Continued on Next Page...

Table 4.1 – Continued

| *FUSE* ID | Object Name | *FUSE* Aperture | RA | Dec | Spectral Type | V mag. | Reference |
|---|---|---|---|---|---|---|---|
| A1330123 | SK-67D166 | LWRS | 05 31 44.31 | -67 38 00.6 | O4If+ | 12.27 | [326] |
| B0860901 | SK-67D168 | MDRS | 05 31 52.10 | -67 34 20.8 | O8Iaf | 12.08 | [336] |
| D9042002 | SNR0532-675 | LWRS | 05 32 23.00 | -67 31 02.0 | Supernova-remnant | | |
| P1173101 | SK-67D191 | LWRS | 05 33 34.12 | -67 30 19.6 | O8V | 13.46 | [327] |
| B0770302 | HV5936 | LWRS | 05 33 39.00 | -66 37 39.8 | B0-B2V-IV | 14.8 | [325] |
| P1175101 | Sk-69D191 | LWRS | 05 34 19.39 | -69 45 10.0 | WC4 | 13.35 | [337] |
| F3210301 | J053441-693139 | LWRS | 05 34 41.30 | -69 31 39.0 | O2-O3.5If* | 13.7 | [338] |
| P1171603 | Sk-67D211 | LWRS | 05 35 13.92 | -67 33 27.0 | O2III(f)* | 12.28 | [338] |
| Z9051001 | BREY64 | LWRS | 05 35 54.45 | -68 59 07.4 | WN9h | 13.21 | [328] |
| D9043101 | SNR0536-692 | LWRS | 05 36 07.70 | -69 11 52.6 | Supernova-remnant | | |
| Z9050701 | SK-69_220 | LWRS | 05 36 43.83 | -69 29 47.4 | WNorOiafpe | 10.58 | [326] |
| P1172201 | Sk-66D172 | LWRS | 05 37 05.56 | -66 21 35.7 | O2III(f)*+OB | 13.13 | [338] |
| C0020601 | BI253 | LWRS | 05 37 34.49 | -69 01 09.8 | Of | 13.76 | [328] |
| E5114201 | SK-68D137 | LWRS | 05 38 24.77 | -68 52 32.8 | O3IIIf | 13.29 | [328] |
| P1171803 | MK42 | LWRS | 05 38 42.10 | -69 05 54.7 | O3If/WN6-A | 10.96 | [339] |
| P1031706 | SK-69D243 | LWRS | 05 38 42.57 | -69 06 03.2 | WN5+OB | 9.5 | [340] |
| F9140101 | 30DOR-S-R136 | LWRS | 05 38 51.70 | -69 06 00.0 | HII-region | | |
| P1031802 | SK-69D246 | LWRS | 05 38 53.50 | -69 02 00.7 | WN | 11.16 | [329] |
| P1174601 | HDE269927 | LWRS | 05 38 58.25 | -69 29 19.1 | WN | 12.63 | [329] |
| P2170101 | SK-69D257 | LWRS | 05 39 58.91 | -69 44 03.2 | O9II | 12.53 | [325] |
| D9042801 | SNR0543-689 | LWRS | 05 43 07.20 | -68 58 52.0 | Supernova-remnant | | |
| D0981401 | D301-1005 | MDRS | 05 43 08.30 | -67 50 52.4 | O9.5V | 14.11 | [328] |
| D0981201 | SK-67D250 | MDRS | 05 43 15.48 | -67 51 09.6 | O7.5II(f) | 12.68 | [341] |
| D0981501 | D301-NW8 | MDRS | 05 43 15.96 | -67 49 51.0 | D301-NW8 | 14.37 | [328] |
| I8120701 | SK-70D115 | LWRS | 05 48 49.76 | -70 03 57.5 | O6.5Iaf | 12.24 | [325] |

Notes. Units of right ascension are hours, minutes, and seconds; units of declination are in degrees, arcminutes, and arcseconds.

Another source of error in the O VI column density measurements is contamination by absorption from molecular hydrogen. The contamination by molecular hydrogen absorption in the LMC velocity range is not significant [312, 320] but may give rise to significant error in the MW velocity. The $H_2$ absorption feature are usually not a problem for measurements of O VI absorption at velocities more than 20 km $s^{-1}$ apart ([343] and references therein). The contamination by $H_2$ in the O VI column density measurements have been estimated for the MW. This is done by fitting the 6-0 P(3) 1031.20 Å and 6-0 R(4) 1032.35 Å transition line of $H_2$ , which are close to the O VI line. The theoretical $H_2$ absorption profiles are subtracted from the *FUSE* data before the calculation of O VI column densities for all sight lines.

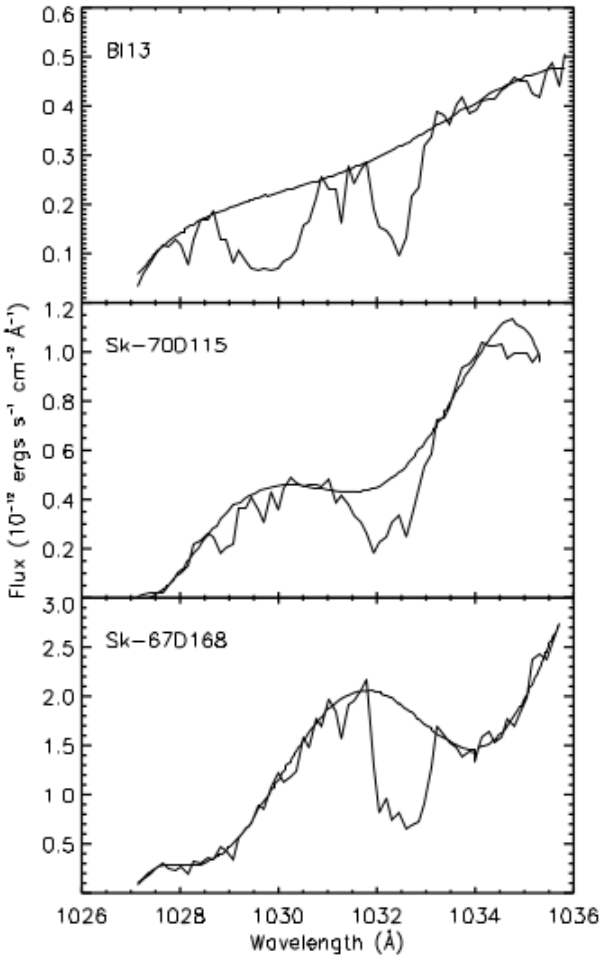


**Figure 4.1:** Complex behaviour of three lines of sight near O VI absorption (1032Å) while fitting continuum. (figure reproduced from Pathak et al. [312]).

### 4.3.2 Apparent Optical Depth Measurements

Here the apparent optical depth (AOD) technique [320, 342, 344] has been used to measure the equivalent width and column density of the O VI absorption. This method uses an apparent optical depth ($\tau_a$) in terms of velocity which is defined as,

$$\tau_a(v) = ln[I_o(v)/I_{obs}(v)], \tag{4.1}$$

where, $I_o$ is the continuum intensity and $I_{obs}$ is the absorption line intensity in terms of velocity. The FWHM of the absorption line is low as compared to the high resolution of the *FUSE*. This makes the apparent optical depth a reliable approximation of the true optical depth. The apparent column density ($N_a(v)$ [atoms cm$^{-2}$ (km s$^{-1}$)$^{-1}$]) is calculated by the following relation

$$N_a(v) = \frac{m_e c \tau_a(v)}{\pi e^2 f \lambda} = 3.768 \times 10^{14} \frac{\tau_a(v)}{f\lambda}, \quad (4.2)$$

where $m_e$ is the mass of the electron, $c$ is the speed of light, $e$ is the electronic charge, $\lambda$ is the line wavelength (in Å) and $f$ is the oscillator strength$f$ of ions (for O VI, $f$ = 0.1325 has been taken from Yan et al. [345]). *FUSE* can completely resolve the broad 1032 Å O VI profile. However, the weaker of the O VI doublet at 1037.6 Å is difficult to separate from the CII* absorption.

Table 4.2 lists the derived equivalent widths and column densities for the MW. The errors in the equivalent widths and column densities are $1\sigma$ uncertainties derived using the uncertainty in the *FUSE* data and the fitting procedures. Apart from the $1\sigma$ uncertainties, the major source of error is the overlap of the MW O VI absorption profile with the LMC O VI absorption. In the column density measurements for the MW, the lower velocity limit of the LMC as considered by Pathak et al. [312] have been adopted to be the upper velocity for the MW. Column 2 of Table 4.2 is the range of velocities over which the absorption profile is integrated to yield the measurements.

In Table 4.2, we also include corresponding LMC results as measured by Pathak et al. [312]. Out of the 70 sight lines, in some cases the MW and LMC O VI absorption profiles overlap. However the separation is quite clear for the sight lines Sk-65D21, Sk-67D69, Sk-65D105, HV2543, Sk-66D100, HV5936, Sk-67D211, Sk-69D220, Sk-66D172, Sk-68D137 and D301-1005.

From Figure 4.2 it is evident that nearly for all O V absorption profiles there exist significant contributions of IVCs and/or HVCs. In order to remove the HVCs, O VI column densities have also been measured by integrating over $|v| \leq 100$ km s$^{-1}$ for all 70 sight lines. The results are presented in Table 4.3.

## 4.4 O VI Column Density

This work covers a large sample of 70 sight lines covering a wide range of targets: O- and B-type stars, Wolf-Rayet objects, supernova remnants etc. The large sample size are definitely helpful in studying the properties and distribution of O VI in the MW.

Significant variation in the O VI column densities in the MW has been observed. The integrated MW O VI column densities log N(O VI) for the total velocity range is found in the range from 13.68 to 14.73 (in units of atoms cm$^{-2}$) which mean a factor of ∼11. The mean MW O VI column density is found to be 14.29 atoms cm$^{-2}$. The

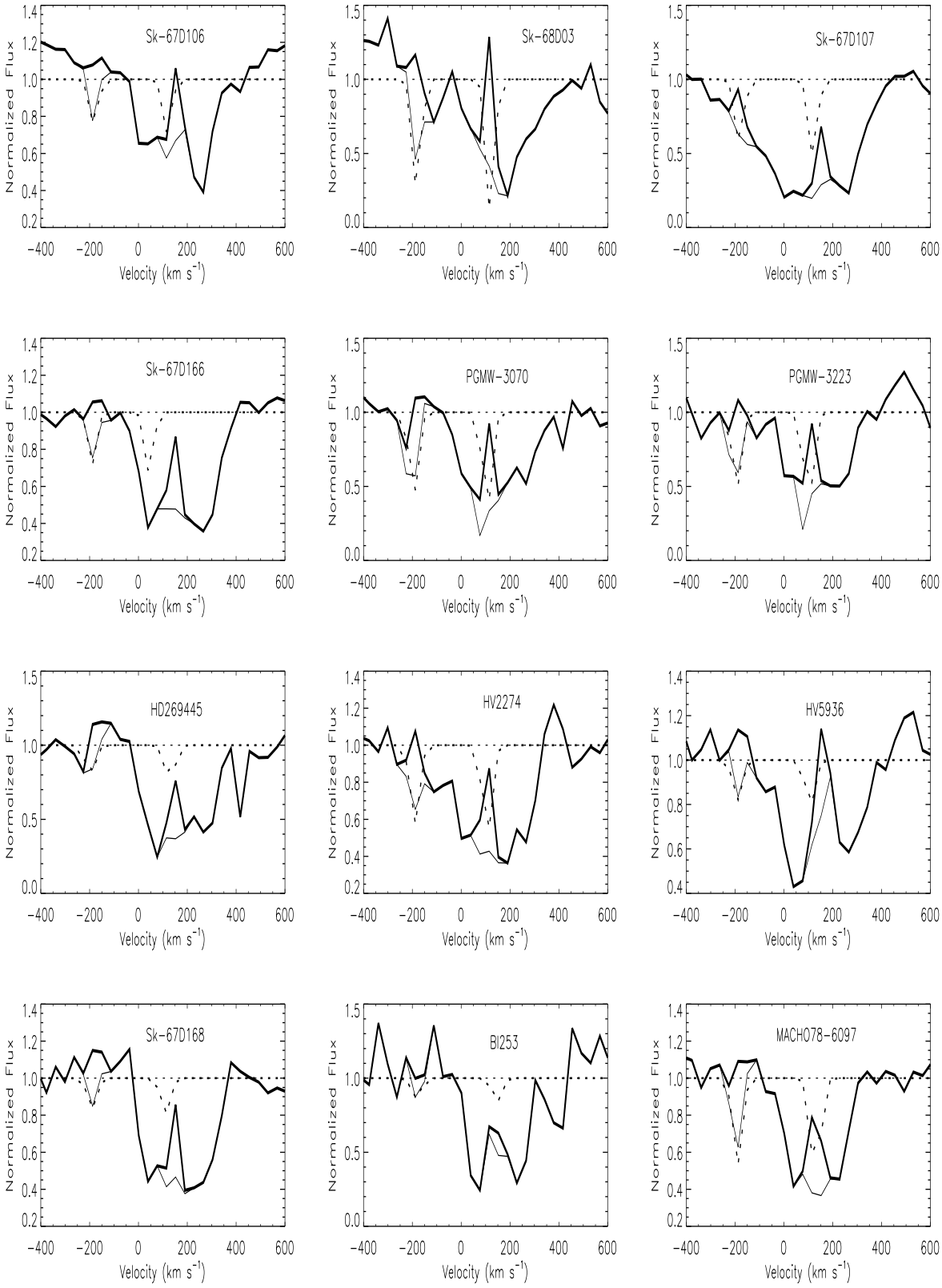


**Figure 4.2:** O VI absorption profiles for 70 lines of sight in the MW. Absorption line profiles of O VI before (thin line) and after (thick line) removal of $H_2$ contamination are shown. Model for $H_2$ absorption (dotted line) for the 70 lines of sight are also shown.

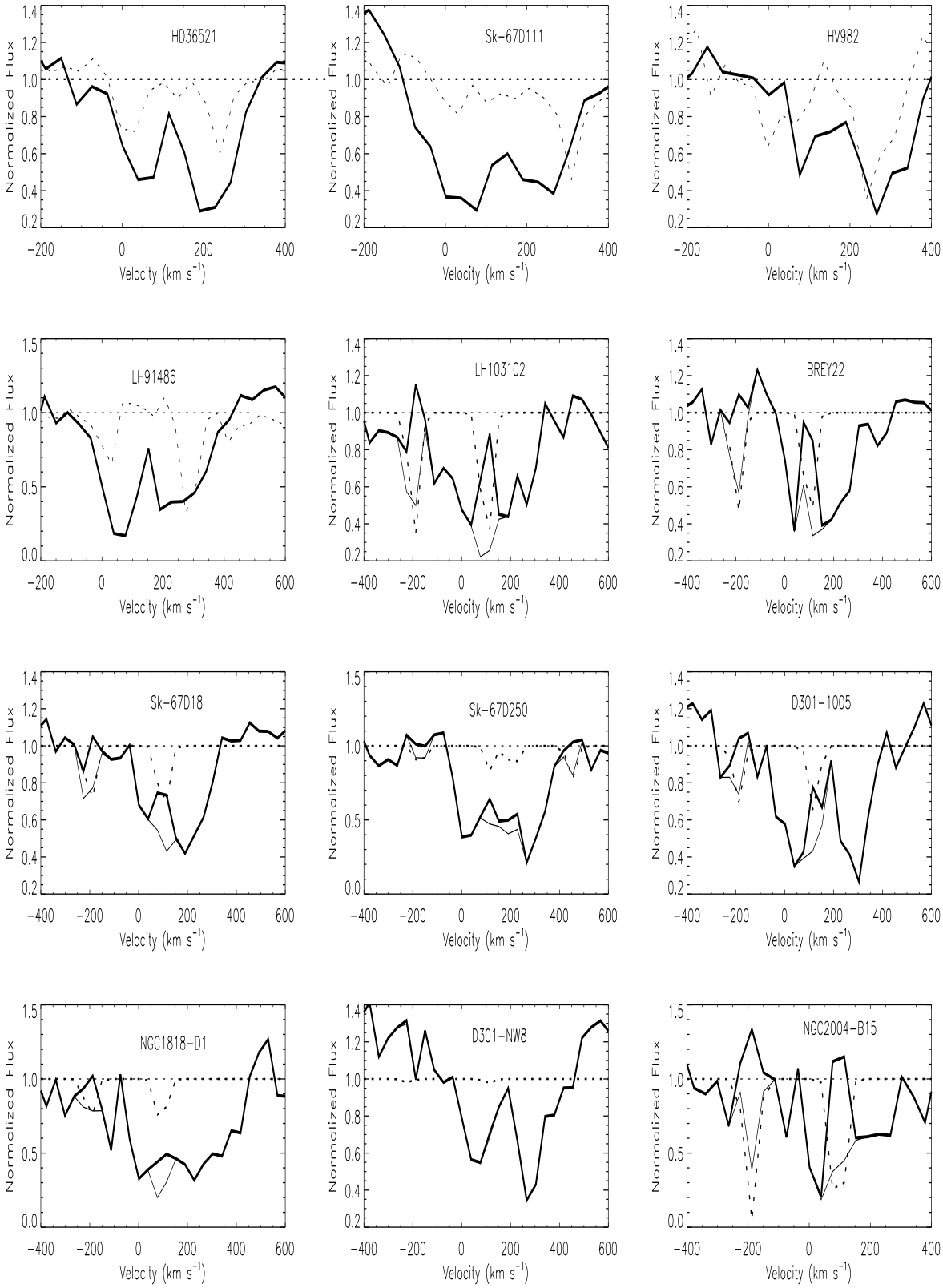


Figure 4.2- *continued*

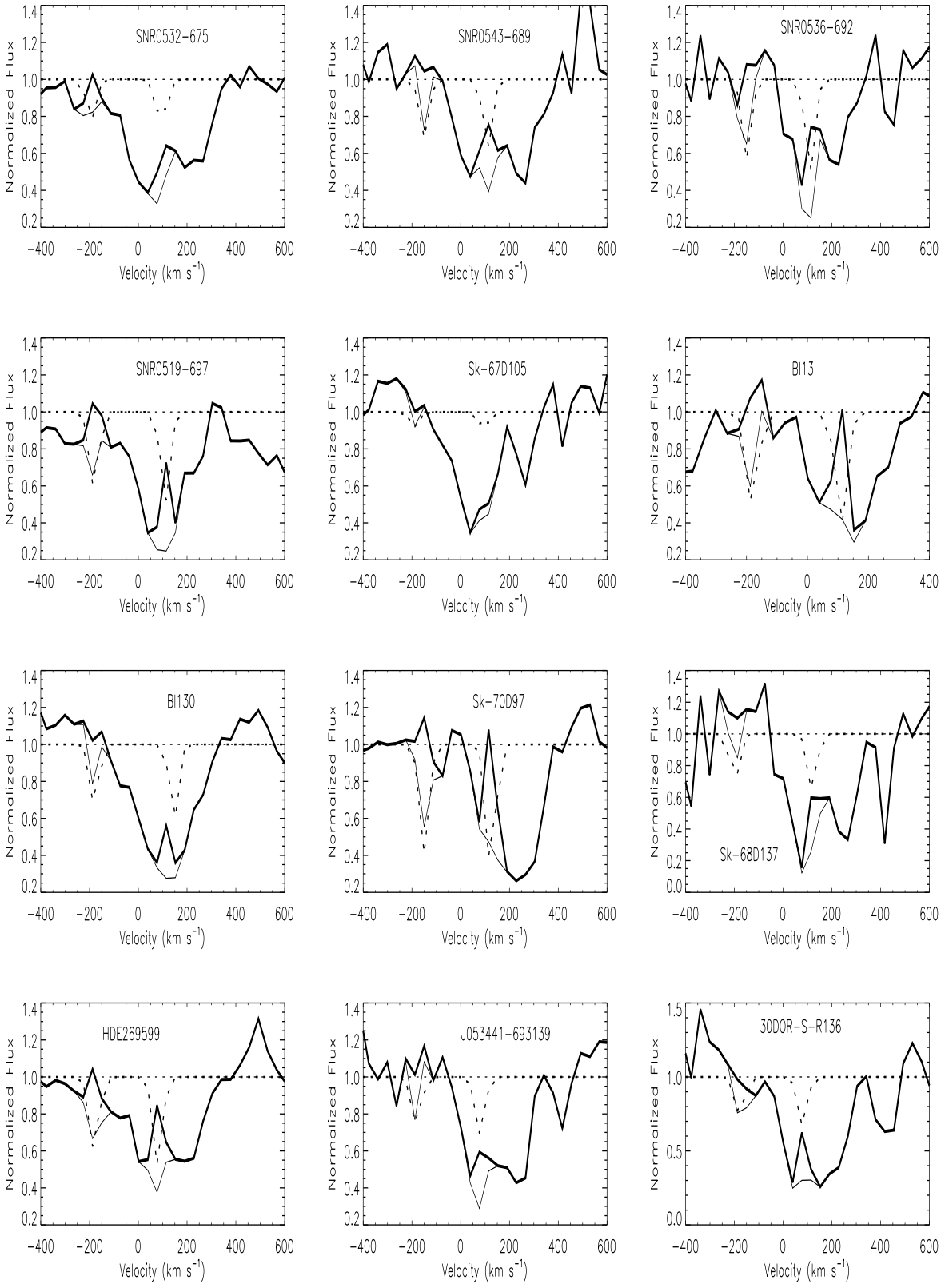


Figure 4.2- *continued*

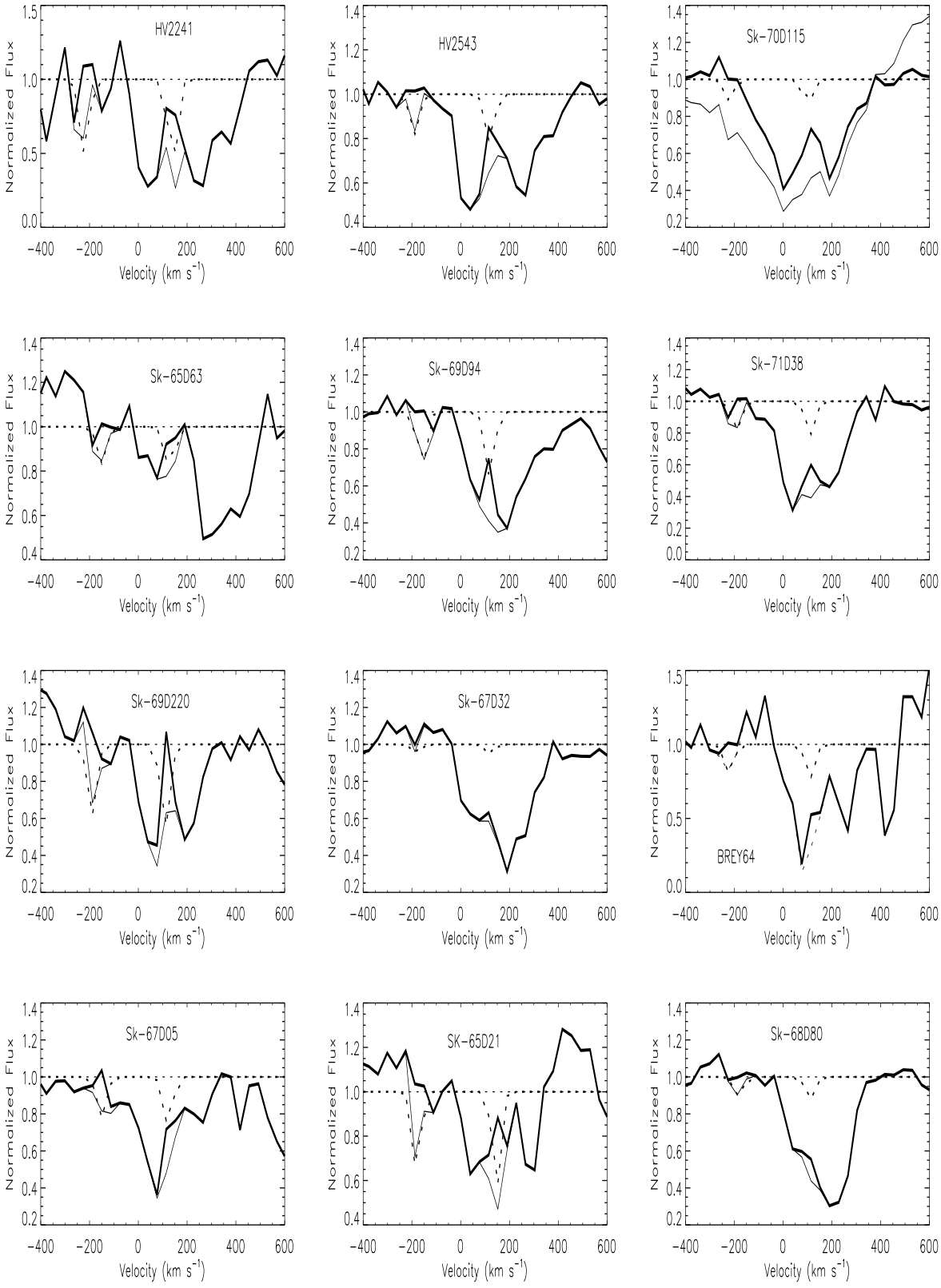


Figure 4.2- *continued*

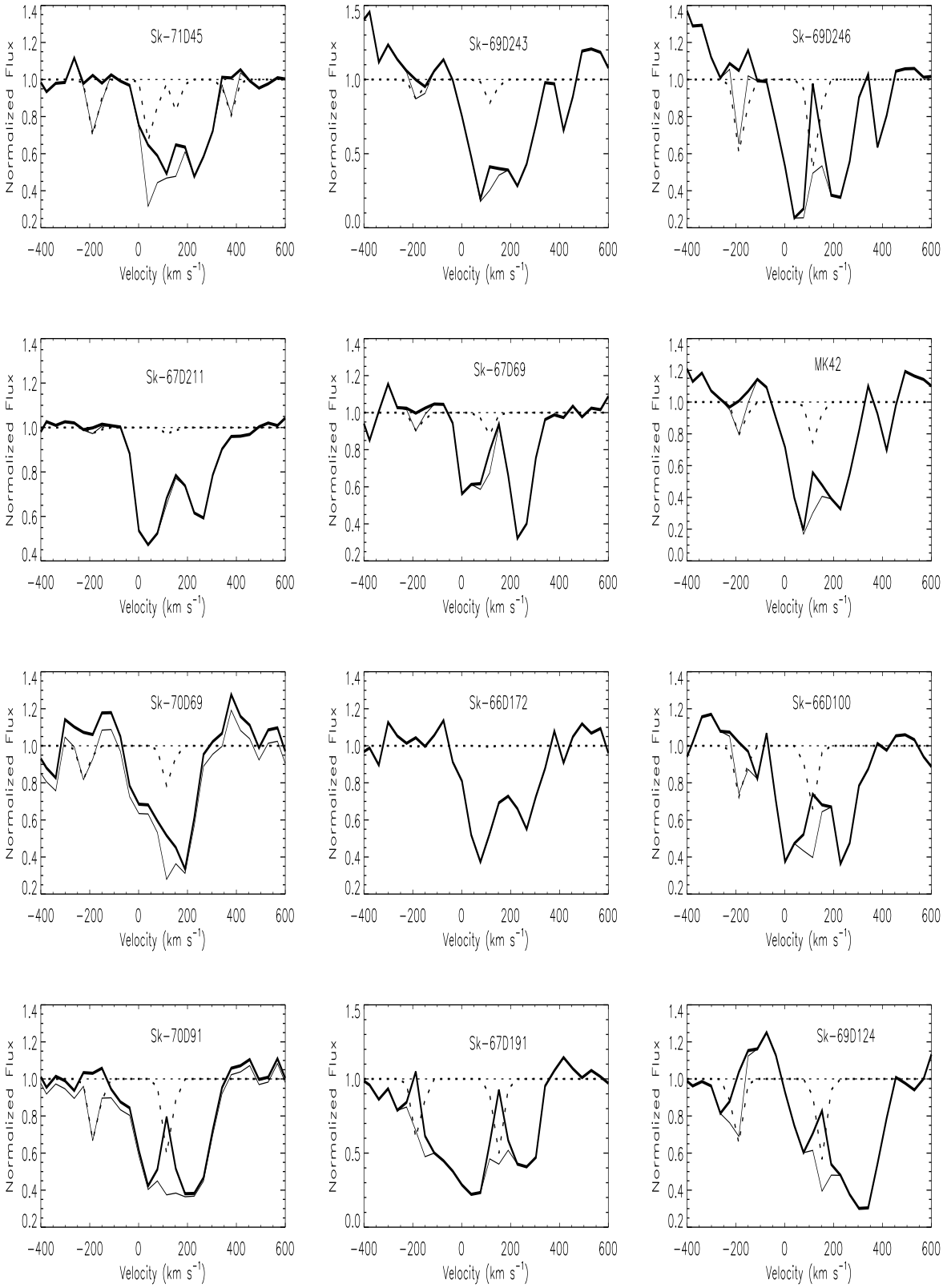


Figure 4.2- *continued*

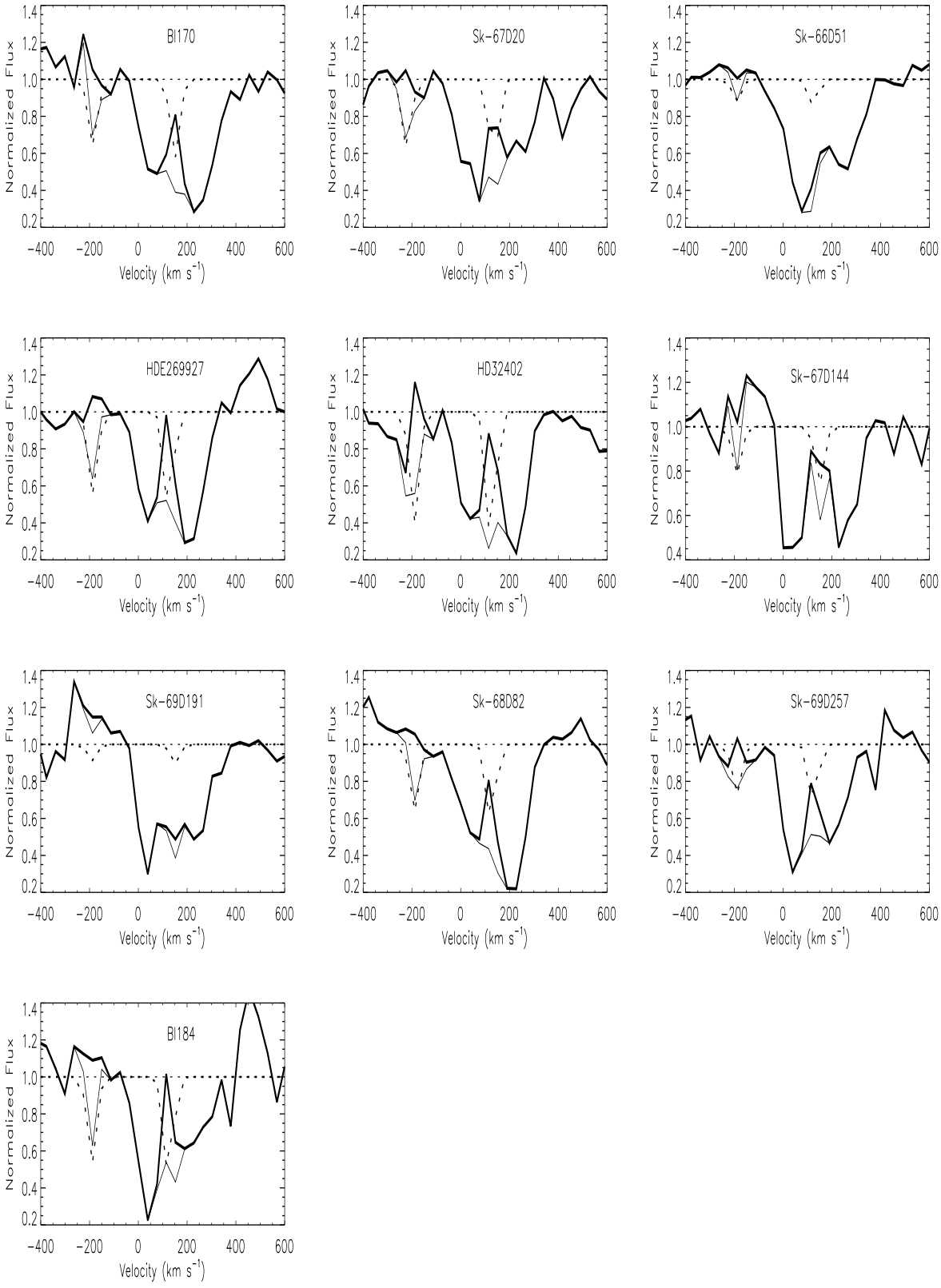


Figure 4.2- *continued*

median value of our sample is 14.21 atoms cm$^{-2}$. The projections of the total column densities perpendicular to the Galactic plane, log (N sin $|b|$) has also been measured. This varies from 13.42 to 14.50 with average and median values of 14.03 and 14.04 atoms cm$^{-2}$ respectively. Earlier using *FUSE* spectra of 11 active galactic nuclei Savage et al. [307] found O VI column density log [N(O VI sin $|b|$] in the MW halo varying from 13.80 to 14.64, with mean and median values of 14.29 and 14.21 atoms cm$^{-2}$ respectively. The O VI column density in the Galactic halo has been measured as log N(O VI) = $14.52^{+0.10}_{-0.14}$ atoms cm$^{-2}$ toward 12 early type stars in the LMC By Howk et al. [306]. The variation of O VI column density reported by Howk et al. [306] when integrated over total velocity range is 14.22 to 14.67 atoms cm$^{-2}$. Studying the *FUSE* spectra of 22 Galactic halo stars, Zsargó J. et al. [346] found column density N(O VI) = 14.17±0.28 atoms cm$^{-2}$ with a variation from 13.65 to 14.57 and log (N sin $|b|$) variation from 13.13 to 14.48. O VI column density in the local interstellar medium for 39 white dwarfs as observed by *FUSE* was reported by Savage et al. [310] with a variation of log N(O VI) = 12.38 to 13.60 giving a median value of 13.10 atoms cm$^{-2}$.

Bowen et al. [319] measured O VI column density for 148 stars and found values in the range $0.08\times10^{14}$ to $4.76\times10^{14}$ atoms cm$^{-2}$. O VI column density variation in the range from 13.23 to 15.03 along with other species for 139 sight lines have been reported with median and average value of log N(O VI) 14.15 and 14.11 atoms cm$^{-2}$ respectively in the Galactic halo by Savage & Wakker [347].

As discussed in section 4.3.2, nearly in all O VI profiles, there are significant contributions from HVC and/or IVCs. In order to exclude much of the HVC components, the MW O VI column densities have also been derived by integrating over $|v| \leq 100$ km s$^{-1}$ which is presented in Table 4.3. The log N(O VI) for these velocity range i.e. from lower to 100 km s$^{-1}$, varies from 14.63 to 13.36 atoms cm$^{-2}$. The mean column density log N(O VI) in this case is 14.24 atoms cm$^{-2}$. Out of the all 70 sight lines, it is found that in case of BREY22 and HDE269599 the two corresponding column density values i.e in the two different velocity ranges are exactly the same. From Figure 4.2 it is evident that these particular sight lines are not extended up to or beyond this velocity i.e. 100 km s$^{-1}$. For the sample (except for BREY22 and HDE269599), it has been seen that the O VI column density contribution from region >100 km s$^{-1}$ is significant. There are 13 cases where the column density contribution is $\geq$ 20%. The highest contribution from these region is found in case of Sk-71D45 (37.83 %).

**Table 4.2:** O VI column densities, equivalent widths and the corresponding velocity limits in the Milky Way and the LMC.

| Target Name | Milky Way | | | LMC | | |
|---|---|---|---|---|---|---|
| | Limit (km s$^{-1}$) | EW (mÅ) | log N(O VI) (dex) | Limit (km s$^{-1}$) | EW (mÅ) | log N(O VI) (dex) |
| SK-67D05 | -30,175 | 259.9±15 | $14.26^{+0.02}_{-0.04}$ | 175, 330 | 73±6 | $13.72^{+0.03}_{-0.03}$ |
| SK-68D03 | -20,120 | 173.5±35 | $14.06^{+0.04}_{-0.04}$ | 180,330 | 112±8 | $14.02^{+0.02}_{-0.03}$ |
| BI13 | -35,120 | 190.0±27 | $14.25^{+0.06}_{-0.08}$ | 175, 315 | 88±4 | $13.94^{+0.02}_{-0.01}$ |
| SK-67D18 | -30,135 | 120.3±30 | $14.12^{+0.12}_{-0.18}$ | 165, 330 | 132±7 | $14.16^{+0.01}_{-0.02}$ |
| Sk-67D20 | -30,175 | 200.2±3 | $14.19^{+0.06}_{-0.07}$ | 175, 335 | 147±8 | $14.08^{+0.01}_{-0.02}$ |
| PGMW-3070 | -50,120 | 131.2±24 | $14.23^{+0.12}_{-0.16}$ | 180, 345 | 132±23 | $14.10^{+0.02}_{-0.02}$ |
| LH103102 | -20,150 | 287.0±23 | $14.38^{+0.02}_{-0.02}$ | 180, 330 | 132±23 | $14.16^{+0.01}_{-0.02}$ |
| LH91486 | -30,175 | 459.9±22 | $14.73^{+0.05}_{-0.06}$ | 175, 385 | 266±29 | $14.47^{+0.01}_{-0.01}$ |
| PGMW-3223 | -50,120 | 128.9±28 | $14.01^{+0.06}_{-0.07}$ | 175, 315 | 129±15 | $14.10^{+0.02}_{-0.02}$ |
| HV2241 | -35,165 | 330.0±79 | $14.56^{+0.05}_{-0.06}$ | 165, 365 | 271±18 | $14.50^{+0.02}_{-0.01}$ |
| HD32402 | -40,140 | 223.5±39 | $14.40^{+0.07}_{-0.09}$ | 160, 320 | 271±3 | $14.48^{+0.01}_{-0.01}$ |
| SK-67D32 | -40,165 | 237.6±6 | $14.35^{+0.06}_{-0.07}$ | 165, 360 | 129±7 | $14.11^{+0.01}_{-0.02}$ |
| SK-65D21 | -20,165 | 95.8±29 | $13.91^{+0.08}_{-0.09}$ | 225, 340 | 94±5 | $13.94^{+0.01}_{-0.02}$ |
| HV2274 | -20,125 | 219.0±20 | $14.19^{+0.09}_{-0.11}$ | 165, 345 | 160±11 | $14.14^{+0.01}_{-0.02}$ |
| Sk-66D51 | -30,170 | 391.8±21 | $14.53^{+0.01}_{-0.01}$ | 170, 370 | 185±10 | $14.26^{+0.01}_{-0.02}$ |
| NGC1818-D1 | -50,150 | 260±75 | $14.46^{+0.03}_{-0.03}$ | 150, 340 | 280±13 | $14.52^{+0.02}_{-0.02}$ |
| SK-70D69 | -50,150 | 160.2±38 | $14.14^{+0.18}_{-0.13}$ | 150, 295 | 182±12 | $14.18^{+0.02}_{-0.02}$ |
| Sk-67D69 | -20,170 | 232.1±45 | $14.18^{+0.08}_{-0.10}$ | 170, 340 | 232±28 | $14.40^{+0.01}_{-0.02}$ |
| MACHO78-6097 | -30,165 | 236.9±52 | $14.32^{+0.04}_{-0.06}$ | 165, 320 | 151±9 | $14.15^{+0.02}_{-0.01}$ |
| BI130 | -30,165 | 339.9±6 | $14.51^{+0.05}_{-0.05}$ | 165, 320 | 94±7 | $13.89^{+0.02}_{-0.03}$ |
| SK-69D94 | -20,160 | 149.8±8 | $14.22^{+0.06}_{-0.06}$ | 160, 340 | 150±3 | $14.22^{+0.02}_{-0.02}$ |
| SNR0519-697 | 2,160 | 339.0±138 | $14.44^{+0.11}_{-0.13}$ | 160, 300 | 97±4 | $13.97^{+0.02}_{-0.02}$ |
| BREY22 | 10,160 | 105.6±21 | $13.94^{+0.08}_{-0.10}$ | 160, 330 | 126±7 | $14.07^{+0.01}_{-0.02}$ |
| HD269445 | -30,175 | 301.2±31 | $14.49^{+0.02}_{-0.02}$ | 175, 365 | 200±10 | $14.29^{+0.01}_{-0.02}$ |
| SK-69D124 | -35,190 | 126.4±38 | $13.95^{+0.08}_{-0.13}$ | 190, 430 | 331±6 | $14.57^{+0.01}_{-0.01}$ |
| SK-67D105 | -40,180 | 311.3±40 | $14.42^{+0.05}_{-0.05}$ | 180, 320 | 110±8 | $13.92^{+0.02}_{-0.03}$ |
| SK-67D106 | -20,150 | 113.0±24 | $13.81^{+0.15}_{-0.22}$ | 175, 345 | 180±6 | $14.30^{+0.01}_{-0.02}$ |
| SK-67D107 | -40,120 | 427.6±2 | $14.63^{+0.03}_{-0.03}$ | 160, 360 | 254±9 | $14.45^{+0.01}_{-0.01}$ |
| HD36521 | -30,175 | 202.2±4 | $14.24^{+0.13}_{-0.19}$ | 175, 340 | 126±9 | $14.07^{+0.01}_{-0.01}$ |
| SK-68D80 | -30,165 | 165.2±3 | $14.08^{+0.04}_{-0.04}$ | 145, 335 | 303±16 | $14.56^{+0.01}_{-0.01}$ |
| SK-68D82 | -20,165 | 226.6±12 | $14.30^{+0.08}_{-0.09}$ | 165, 320 | 141±10 | $14.17^{+0.01}_{-0.01}$ |
| BI170 | -35,165 | 221.1±55 | $14.38^{+0.02}_{-0.02}$ | 165, 365 | 235±7 | $14.43^{+0.01}_{-0.02}$ |
| SK-67D111 | -30,175 | 329.3±40 | $14.46^{+0.05}_{-0.05}$ | 175, 365 | 214±19 | $14.34^{+0.02}_{-0.01}$ |
| HV2543 | -35,160 | 230.6±25 | $14.30^{+0.07}_{-0.12}$ | 160, 365 | 156±8 | $14.23^{+0.02}_{-0.01}$ |
| SK-70D91 | -45,160 | 223.6±44 | $14.39^{+0.04}_{-0.04}$ | 160, 365 | 256±7 | $14.43^{+0.02}_{-0.01}$ |
| Sk-66D100 | -35,160 | 345.2±39 | $14.46^{+0.05}_{-0.06}$ | 160, 340 | 214±21 | $14.34^{+0.02}_{-0.02}$ |
| HDE269599 | -40,100 | 169.6±21 | $14.18^{+0.04}_{-0.05}$ | 165, 320 | 123±6 | $14.05^{+0.02}_{-0.02}$ |
| SK-65D63 | -40,150 | 54.0±19 | $13.68^{+0.16}_{-0.25}$ | 180, 375 | 184±8 | $14.21^{+0.02}_{-0.02}$ |
| HV982 | 40,175 | 117.5±55 | $13.91^{+0.07}_{-0.11}$ | 175, 360 | 208±6 | $14.33^{+0.01}_{-0.01}$ |

Continued on Next Page...

Table 4.2 – Continued

| Target Name | Milky Way | | | LMC | | |
|---|---|---|---|---|---|---|
| | Limit (km $s^{-1}$) | EW (mÅ) | log N(O VI) (dex) | Limit (km $s^{-1}$) | EW (mÅ) | log N(O VI) (dex) |
| SK-70D97 | 20,175 | 74.9±12 | $13.74^{+0.10}_{-0.12}$ | 175, 375 | 226±4 | $14.39^{+0.01}_{-0.02}$ |
| Sk-67D144 | -30,165 | 185.2±76 | $14.19^{+0.06}_{-0.07}$ | 165, 335 | 194±10 | $14.25^{+0.01}_{-0.02}$ |
| BI184 | -30,165 | 295.4±28 | $14.51^{+0.03}_{-0.05}$ | 165, 330 | 118±10 | $14.04^{+0.03}_{-0.03}$ |
| NGC2004-B15 | -30,165 | 200.5±24 | $14.22^{+0.09}_{-0.12}$ | 175, 330 | 92±7 | $13.86^{+0.01}_{-0.03}$ |
| SK-71D38 | -50,165 | 350.1±21 | $14.52^{+0.04}_{-0.04}$ | 165, 315 | 94±7 | $13.92^{+0.02}_{-0.03}$ |
| Sk-71D45 | -30,160 | 283.0±26 | $14.38^{+0.08}_{-0.01}$ | 160, 345 | 194±9 | $14.26^{+0.02}_{-0.01}$ |
| SK-67D166 | -20,165 | 260.0±21 | $14.29^{+0.04}_{-0.04}$ | 165, 390 | 206±2 | $14.32^{+0.02}_{-0.01}$ |
| SK-67D168 | -30,165 | 149.2±40 | $14.27^{+0.02}_{-0.03}$ | 165, 375 | 186±12 | $14.26^{+0.02}_{-0.02}$ |
| SNR0532-675 | -70,165 | 422±190 | $14.51^{+0.05}_{-0.09}$ | 165, 345 | 147±9 | $14.16^{+0.02}_{-0.02}$ |
| SK-67D191 | -40,165 | 462.7±27 | $14.64^{+0.01}_{-0.01}$ | 165, 340 | 127±6 | $14.08^{+0.02}_{-0.02}$ |
| HV5936 | -30,175 | 286.0±25 | $14.41^{+0.04}_{-0.05}$ | 175, 375 | 174±8 | $14.18^{+0.02}_{-0.02}$ |
| Sk-69D191 | -30,165 | 219.0±44 | $14.22^{+0.04}_{-0.04}$ | 165, 340 | 185±11 | $14.22^{+0.02}_{-0.01}$ |
| J053441-693139 | -35,165 | 189.7±63 | $14.18^{+0.15}_{-0.25}$ | 165, 330 | 182±5 | $14.22^{+0.01}_{-0.01}$ |
| Sk-67D211 | -40,160 | 317.0±19 | $14.45^{+0.06}_{-0.08}$ | 160, 350 | 144±8 | $14.11^{+0.02}_{-0.02}$ |
| BREY64 | 10,180 | 239.0±43 | $14.25^{+0.16}_{-0.25}$ | 180, 330 | 139±8 | $14.20^{+0.02}_{-0.01}$ |
| SNR0536-692 | 38, 165 | 139.7±39.7 | $14.16^{+0.07}_{-0.07}$ | 165, 320 | 116±7 | $14.03^{+0.05}_{-0.07}$ |
| SK-69D220 | -40,155 | 222.0±23 | $14.33^{+0.03}_{-0.02}$ | 160, 315 | 128±9 | $14.09^{+0.02}_{-0.03}$ |
| Sk-66D172 | -30,175 | 316.9±38 | $14.47^{+0.03}_{-0.03}$ | 175, 360 | 173±9 | $14.20^{+0.02}_{-0.01}$ |
| BI253 | -20,160 | 260.0±46 | $14.36^{+0.04}_{-0.05}$ | 160, 300 | 259±9 | $14.46^{+0.01}_{-0.01}$ |
| SK-68D137 | -20,165 | 307.0±51 | $14.37^{+0.05}_{-0.06}$ | 165, 330 | 234±7 | $14.45^{+0.01}_{-0.01}$ |
| MK42 | -20,160 | 367.4±12 | $14.48^{+0.09}_{-0.11}$ | 160, 330 | 228±24 | $14.41^{+0.01}_{-0.01}$ |
| SK-69D243 | 10,150 | 293.2±15 | $14.40^{+0.08}_{-0.09}$ | 150, 345 | 307±15 | $14.56^{+0.01}_{-0.01}$ |
| 30DOR-S-R136 | -30,165 | 212.8±45 | $14.16^{+0.10}_{-0.16}$ | 165, 320 | 185±9 | $14.25^{+0.01}_{-0.02}$ |
| SK-69D246 | -40,145 | 358.9±2 | $14.56^{+0.03}_{-0.03}$ | 155, 325 | 211±3 | $14.37^{+0.02}_{-0.01}$ |
| HDE269927 | -40,160 | 228.6±21 | $14.34^{+0.06}_{-0.07}$ | 160, 320 | 245±3 | $14.42^{+0.01}_{-0.02}$ |
| SK-69D257 | -40,160 | 245.8±98 | $14.49^{+0.05}_{-0.06}$ | 160, 315 | 171±8 | $14.20^{+0.02}_{-0.01}$ |
| SNR0543-689 | 0, 160 | 238.8±8.47 | $14.24^{+0.09}_{-0.10}$ | 160, 360 | 186±34 | $14.27^{+0.12}_{-0.10}$ |
| D301-1005 | -30,165 | 279.8±72 | $14.47^{+0.04}_{-0.04}$ | 165, 385 | 284±9 | $14.53^{+0.01}_{-0.01}$ |
| SK-67D250 | -40,165 | 212.8±58 | $14.29^{+0.04}_{-0.05}$ | 165, 375 | 316±7 | $14.57^{+0.01}_{-0.01}$ |
| D301-NW8 | -30, 175 | 204.2±35.5 | $14.29^{+0.02}_{-0.02}$ | 175, 365 | 228±30 | $14.42^{-0.03}_{+0.02}$ |
| SK-70D115 | -40,165 | 170.8±1 | $14.36^{+0.08}_{-0.11}$ | 165, 330 | 186±2 | $14.23^{+0.01}_{-0.02}$ |

Notes. LMC values are taken from Pathak et al.[312]

**Table 4.3:** O VI column densities with the corresponding velocity limits in the Milky Way.

| Target name | limit (km s$^{-1}$) | log N(O VI) (dex) | log N(O VI) HVC removed(dex) |
|---|---|---|---|
| SK-67D05 | -30, 100 | $14.19^{+0.03}_{-0.03}$ | $13.43^{+1.61}_{-1.67}$ |
| SK-68D03 | -20, 100 | $14.03^{+0.01}_{-0.01}$ | $12.81^{+1.14}_{-1.19}$ |
| BI13 | -35, 100 | $14.23^{+0.06}_{-0.07}$ | $12.97^{+0.00}_{-1.71}$ |
| SK-67D18 | -30, 100 | $14.09^{+0.12}_{-0.17}$ | $12.83^{+0.00}_{-1.81}$ |
| Sk-67D20 | -30, 100 | $14.05^{+0.07}_{-0.09}$ | $13.61^{+1.57}_{-1.42}$ |
| PGMW-3070 | -50, 100 | $14.22^{+0.12}_{-0.16}$ | $12.51^{+0.00}_{-0.00}$ |
| LH103102 | -20, 100 | $14.35^{+0.02}_{-0.02}$ | $13.26^{+0.00}_{-0.00}$ |
| LH91486 | -30, 100 | $14.63^{+0.05}_{-0.06}$ | $14.03^{+0.00}_{-0.00}$ |
| PGMW-3223 | -50, 100 | $14.01^{+0.06}_{-0.07}$ | $10.06^{+0.00}_{-0.00}$ |
| HV2241 | -35, 100 | $14.52^{+0.04}_{-0.05}$ | $13.53^{+1.59}_{-1.69}$ |
| HD32402 | -40, 100 | $14.36^{+0.07}_{-0.08}$ | $13.29^{+0.00}_{-1.72}$ |
| SK-67D32 | -40, 100 | $14.20^{+0.06}_{-0.07}$ | $13.82^{+0.00}_{-0.00}$ |
| SK-65D21 | -20, 100 | $13.90^{+0.07}_{-0.09}$ | $12.14^{+0.00}_{-1.56}$ |
| HV2274 | -20, 100 | $14.18^{+0.09}_{-0.12}$ | $12.43^{+1.75}_{-0.00}$ |
| Sk-66D51 | -30, 100 | $14.37^{+0.01}_{-0.01}$ | $14.02^{+0.00}_{-0.00}$ |
| NGC1818-D1 | -50, 100 | $14.45^{+0.03}_{-0.04}$ | $12.69^{+1.67}_{-0.00}$ |
| SK-70D69 | -50, 100 | $14.10^{+0.12}_{-0.18}$ | $13.10^{+0.02}_{-1.51}$ |
| Sk-67D69 | -20, 100 | $14.08^{+0.04}_{-0.04}$ | $13.48^{+0.98}_{-0.93}$ |
| MACHO78-6097 | -30, 100 | $14.29^{+0.05}_{-0.05}$ | $13.21^{+1.59}_{-1.69}$ |
| BI130 | -30, 100 | $14.39^{+0.04}_{-0.05}$ | $13.87^{+0.00}_{-1.59}$ |
| SK-69D94 | -20, 100 | $14.12^{+0.06}_{-0.07}$ | $13.53^{+1.73}_{-0.00}$ |
| SNR0519-697 | 2, 100 | $14.36^{+0.05}_{-0.06}$ | $13.63^{+0.00}_{-0.00}$ |
| BREY22 | 10, 100 | $13.94^{+0.08}_{-0.10}$ | -0- |
| HD269445 | -30, 100 | $14.45^{+0.02}_{-0.03}$ | $13.93^{+0.00}_{-1.66}$ |
| SK-69D124 | -35, 100 | $13.85^{+0.08}_{-0.08}$ | $13.24^{+0.00}_{-1.04}$ |
| SK-67D105 | -40, 100 | $14.39^{+0.05}_{-0.05}$ | $13.20^{+0.00}_{-0.00}$ |
| SK-67D106 | -20, 100 | $13.81^{+0.15}_{-0.24}$ | $10.05^{+0.00}_{-1.57}$ |
| SK-67D107 | -40, 100 | $14.62^{+0.03}_{-0.03}$ | $12.94^{+0.00}_{-0.00}$ |
| HD36521 | -30, 100 | $14.19^{+0.13}_{-0.19}$ | $13.31^{+0.00}_{-0.00}$ |
| SK-68D80 | -30, 100 | $14.05^{+0.04}_{-0.04}$ | $12.94^{+0.00}_{-0.00}$ |
| SK-68D82 | -20, 100 | $14.23^{+0.07}_{-0.09}$ | $13.46^{+0.00}_{-1.56}$ |
| BI170 | -35, 100 | $14.25^{+0.02}_{-0.02}$ | $13.78^{+0.00}_{-0.00}$ |
| SK-67D111 | -30, 100 | $14.43^{+0.05}_{-0.05}$ | $13.20^{+0.00}_{-0.00}$ |
| HV2543 | -35, 100 | $14.27^{+0.07}_{-0.07}$ | $13.12^{+0.00}_{-0.00}$ |
| SK-70D91 | -45, 100 | $14.34^{+0.03}_{-0.04}$ | $13.46^{+0.00}_{-1.60}$ |
| Sk-66D100 | -35, 100 | $14.39^{+0.05}_{-0.05}$ | $13.62^{+1.69}_{-0.00}$ |
| HDE269599 | -40, 100 | $14.18^{+0.04}_{-0.05}$ | -0- |
| SK-65D63 | -40, 100 | $13.36^{+0.20}_{-0.26}$ | $12.90^{+1.89}_{-0.86}$ |
| HV982 | 40, 100 | $13.86^{+0.07}_{-0.08}$ | $12.97^{+1.26}_{-0.00}$ |
| SK-70D97 | 20, 100 | $13.70^{+0.09}_{-0.12}$ | $12.72^{+0.00}_{-1.54}$ |

Continued on Next Page...

Table 4.3 – Continued

| Target name | limit (km $s^{-1}$) | log N(O VI) (dex) | log N(O VI) HVC removed (dex) |
|---|---|---|---|
| Sk-67D144 | -30, 100 | $14.14^{+0.06}_{-0.07}$ | $13.25^{+0.00}_{-0.00}$ |
| BI184 | -30, 100 | $14.48^{+0.04}_{-0.04}$ | $13.25^{+1.68}_{-1.60}$ |
| NGC2004-B15 | -30, 100 | $14.22^{+0.09}_{-0.12}$ | $9.78^{+0.00}_{-0.00}$ |
| SK-71D38 | -50, 100 | $14.49^{+0.04}_{-0.04}$ | $13.39^{+0.00}_{-0.00}$ |
| Sk-71D45 | -30, 100 | $14.17^{+0.08}_{-0.10}$ | $13.95^{+0.00}_{-0.00}$ |
| SK-67D166 | -20, 100 | $14.28^{+0.04}_{-0.04}$ | $12.80^{+0.00}_{-0.00}$ |
| SK-67D168 | -30, 100 | $14.24^{+0.02}_{-0.02}$ | $13.04^{+1.66}_{-0.00}$ |
| SNR0532-675 | -70, 100 | $14.46^{+0.05}_{-0.02}$ | $13.50^{+0.85}_{-1.13}$ |
| SK-67D191 | -40, 100 | $14.55^{+0.01}_{-0.01}$ | $11.28^{+0.00}_{-0.00}$ |
| HV5936 | -30, 100 | $14.34^{+0.04}_{-0.04}$ | $13.59^{+1.68}_{-0.00}$ |
| Sk-69D191 | -30, 100 | $14.22^{+0.04}_{-0.04}$ | $13.90^{+0.00}_{-0.00}$ |
| J053441-693139 | -35, 100 | $14.17^{+0.15}_{-0.23}$ | $12.65^{+1.58}_{-0.00}$ |
| Sk-67D211 | -40, 100 | $14.37^{+0.06}_{-0.06}$ | $13.70^{+1.41}_{-0.00}$ |
| BREY64 | 10, 100 | $14.21^{+0.16}_{-0.25}$ | $13.12^{+0.00}_{-0.00}$ |
| SNR0536-692 | 38, 100 | $14.06^{+0.50}_{-0.22}$ | $13.46^{+1.46}_{-1.11}$ |
| SK-69D220 | -40, 100 | $14.28^{+0.02}_{-0.02}$ | $13.44^{+0.00}_{-1.61}$ |
| Sk-66D172 | -30, 100 | $14.32^{+0.03}_{-0.03}$ | $13.95^{+0.00}_{-0.00}$ |
| BI253 | -20, 100 | $14.34^{+0.04}_{-0.04}$ | $13.02^{+1.68}_{-0.00}$ |
| SK-68D137 | -20, 100 | $14.33^{+0.05}_{-0.06}$ | $13.36^{+0.00}_{-0.00}$ |
| MK42 | -20, 100 | $14.40^{+0.09}_{-0.11}$ | $13.71^{+0.00}_{-0.00}$ |
| SK-69D243 | 10, 100 | $14.32^{+0.07}_{-0.09}$ | $13.64^{+0.00}_{-0.00}$ |
| 30DOR-S-R136 | -30, 100 | $14.16^{+0.12}_{-0.13}$ | $10.40^{+1.31}_{-1.23}$ |
| SK-69D246 | -40, 100 | $14.51^{+0.03}_{-0.03}$ | $13.57^{+0.00}_{-0.00}$ |
| HDE269927 | -40, 100 | $14.32^{+0.05}_{-0.06}$ | $13.12^{+1.70}_{-1.58}$ |
| SK-69D257 | -40, 100 | $14.45^{+0.05}_{-0.05}$ | $13.44^{+1.69}_{-0.00}$ |
| SNR0543-689 | 0, 100 | $14.20^{+0.06}_{-0.07}$ | $13.21^{+1.71}_{-1.57}$ |
| D301-1005 | -30, 100 | $14.41^{+0.04}_{-0.04}$ | $13.56^{+0.00}_{-0.00}$ |
| SK-67D250 | -40, 100 | $14.29^{+0.05}_{-0.04}$ | $11.70^{+0.00}_{-0.00}$ |
| D301-NW8 | -30, 100 | $14.17^{+0.03}_{-0.03}$ | $13.66^{+1.66}_{-1.60}$ |
| SK-70D115 | -40, 100 | $14.35^{+0.07}_{-0.08}$ | $12.68^{+1.26}_{-1.56}$ |

Howk et al. [306] reported O VI column density in the Galactic halo from 13.61 to 14.23 in the velocity range -50 to +50 km $s^{-1}$ and 14.22 to 14.67 when integrated over total velocity range for 12 stars in the LMC. Each individual sight line of the 12 stars gives significantly different column density values for the two corresponding velocity limits.

### 4.4.1 Comparison with the LMC and the SMC

The metallicity of the MW is higher than that of the LMC. This directly implies that the O VI abundance in the MW should be higher compared to that of the LMC. O VI

column density for all the 70 lines toward the LMC have already been reported in details by Pathak et al. [312]. They found high abundance of O VI with log N(O VI) in the range from 13.72 to 14.57 and mean 14.23 atoms $cm^{-2}$ in the LMC. This clearly implies that the order of variation of LMC values is lower then the MW. Also the mean O VI column density for the MW is higher then the LMC. Considering the inclination angle of the LMC to be 33°, Pathak et al. [312] calculated the projected O VI column density on the plane as 14.16. It is found that the MW O VI column densities are indeed higher (or comparable) than the LMC values which are given in Pathak et al. citepPathak et al.11. The properties of O VI absorption profiles are similar as of the LMC which is in agreement to Pathak et al.[312].

Howk et al. [320] analysed the distribution and kinematics of O VI absorption towards 12 early-type stars in the LMC. They observed O VI absorption for all 12 stars and derived column densities in the range log N(O VI) = 13.9-14.6 with the mean of 14.37 atoms $cm^{-2}$. They report that the average column density of O VI and the dispersion of the individual measurements about the mean are identical to those measured for the halo of the MW. From these similarities they suggest that the LMC O VI may arise in a vertically extended distribution similar to the Galactic halo.

Since, the O VI absorption is very patchy in nature and the O VI abundance depends on local ISM conditions, it is extremely difficult to compare the O VI column densities of the MW and the LMC.

O VI absorption in the SMC was surveyed by Hoopes et al. [348] for 18 early-type stars. They reported a widespread presence of O VI with a mean value of N(O VI) 14.53 atoms $cm^{-2}$. Even the metallicity is lower in the SMC, the column density value is higher than the MW and LMC. Highest abundance of O VI has been found at NGC 346 which is a star forming region of the SMC. In the SMC the O VI profile is always shifted to higher velocities than the main component of lower ionization gas traced by Fe II absorption [348].

### 4.4.2 Fe II Absorption and Kinematic Properties of O VI

O VI absorption profiles for the MW and the LMC may be quite different from each other. From Figure 4.2 it is clear that the kinematics of the observed O VI absorption of the MW varies significantly from LMC profiles. As a result it becomes complicated to study their kinematics and provide a comparison. The Fe II absorption at 1125.45 Å compared with the O VI absorption is definitely a better way to study the kinematics [320].

Figure 4.3 shows a comparison of the O VI velocity profiles which are already cleaned of $H_2$ with Fe II profiles. It is well known that Fe II absorptions trace low-ionization gas associated with the relatively high column density warm neutral and warm ionized media. Study of Fe II absorption profiles provide information about MW, IVCs, HVCs, and LMC absorption as clear signatures of these components can be seen.

In most of the cases sharp Fe II absorptions can be seen such as Sk-69D257, Sk-67D211 etc. This feature definitely suggests that the Fe II-bearing material is confined to relatively small distance from the MW midplane.

The shape of the profiles is quite different for some sight lines over the lowest velocities. Except for Sk-70D97, BI253 and HV982 all other sight lines show significant absorption at negative velocities. This is most significant for Sk-67D191, Sk-70D115, SNR0543-689, LH103102, HV2274, HDE269599, Sk-67D105, SNR0519-697, Sk-67D111, Sk-67D107, BI130, SNR0532-675, D01-1005,HV596 and NGC1818-D1. Almost all O VI absorption profiles in the sample are contaminated by IVCs and/or HVCs with few exceptions (i.e. for NGC2004-B15, 30DOR-S-R136 and Sk-65D63). Though these velocity clouds are not seen in the Fe II profiles, weak IVC absorption has been observed for Sk-68D82, Sk-69D191, Sk-69D220, HDE269599 and Sk-70D97. The MW Fe II absorption traces the low velocity edge of the O VI profile and often sharp. The extended O VI absorption towards higher velocities is caused by the strong IVCs and HVCs.

Evidence of IVCs and/or HVCs components in the O VI absorption profiles for LMC can also be seen for all sight lines. In comparison to the Fe II, O VI absorption profiles in the LMC extend to the lower velocities. Almost all Fe II profiles are aligned to the high velocity edge of O VI.

In the direction of the LMC the MW O VI absorption is clearly broader than the Fe II. This definitely indicates that O VI is produced in a layer much more extended than that traced by Fe II and the presence of O VI layer and the Fe II layer are different in the MW.

A clear separation between the MW and LMC O VI absorption has been seen for some sight lines (i.e. for HV5936 etc.). Single Gaussian is fitted to these lines of sights and measured the line width for O VI absorption profiles for the MW. The measured FWHM values for these sight lines are 130, 63, 148, 142, 120, 124, 159, 118, 104, 140, 98 and 115 km $s^{-1}$ respectively. This gives the temperature for the O VI absorbing region in the range $\sim (1.3-8.8)\times10^6$ K. This suggest that the observed FWHM is much higher as in collisional ionization equilibrium (CIE) O VI peaks at $2.8\times10^5$ K. There may be

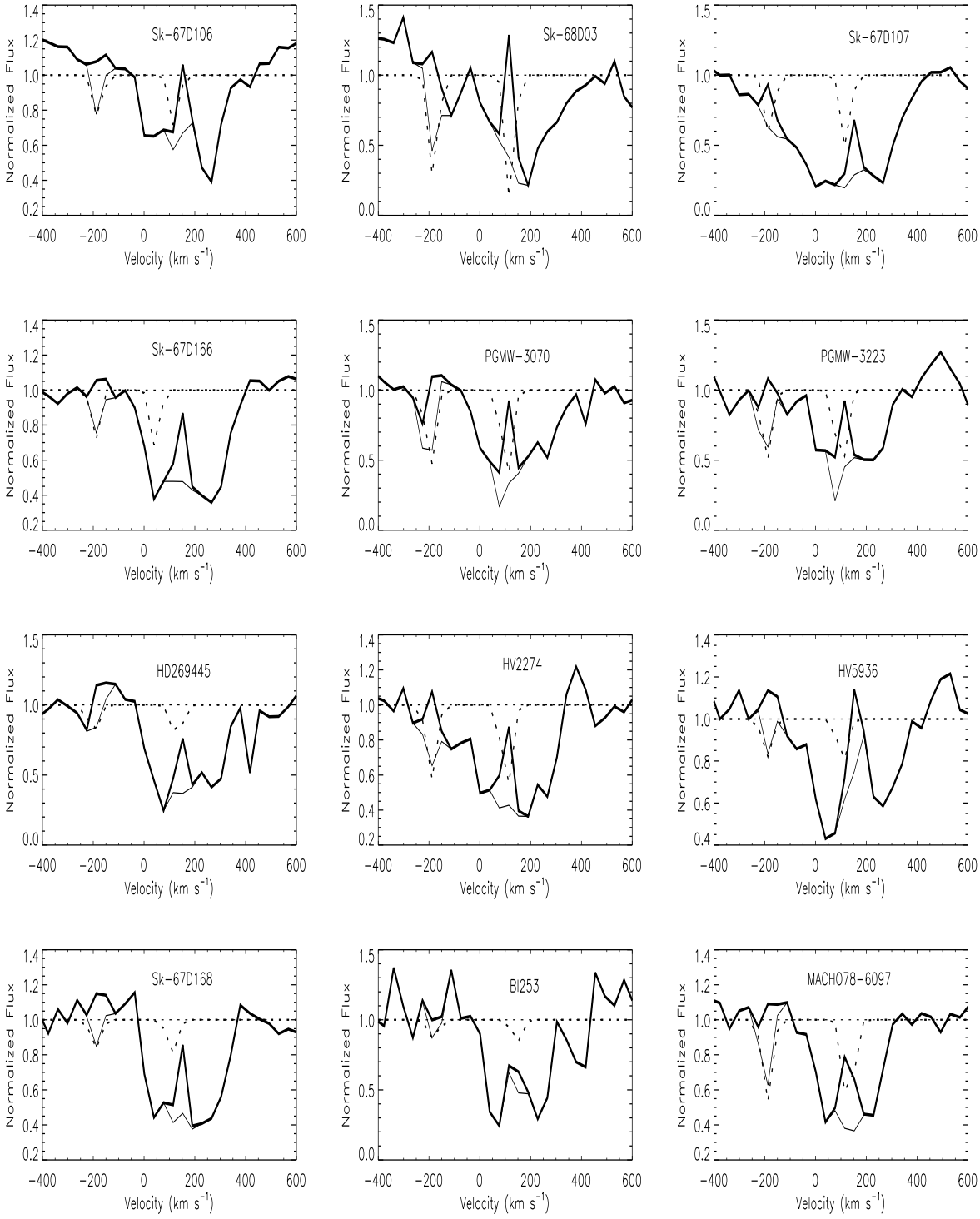


**Figure 4.3:** O VI absorption profiles for 70 lines of sight along with Fe II components in the MW and LMC.

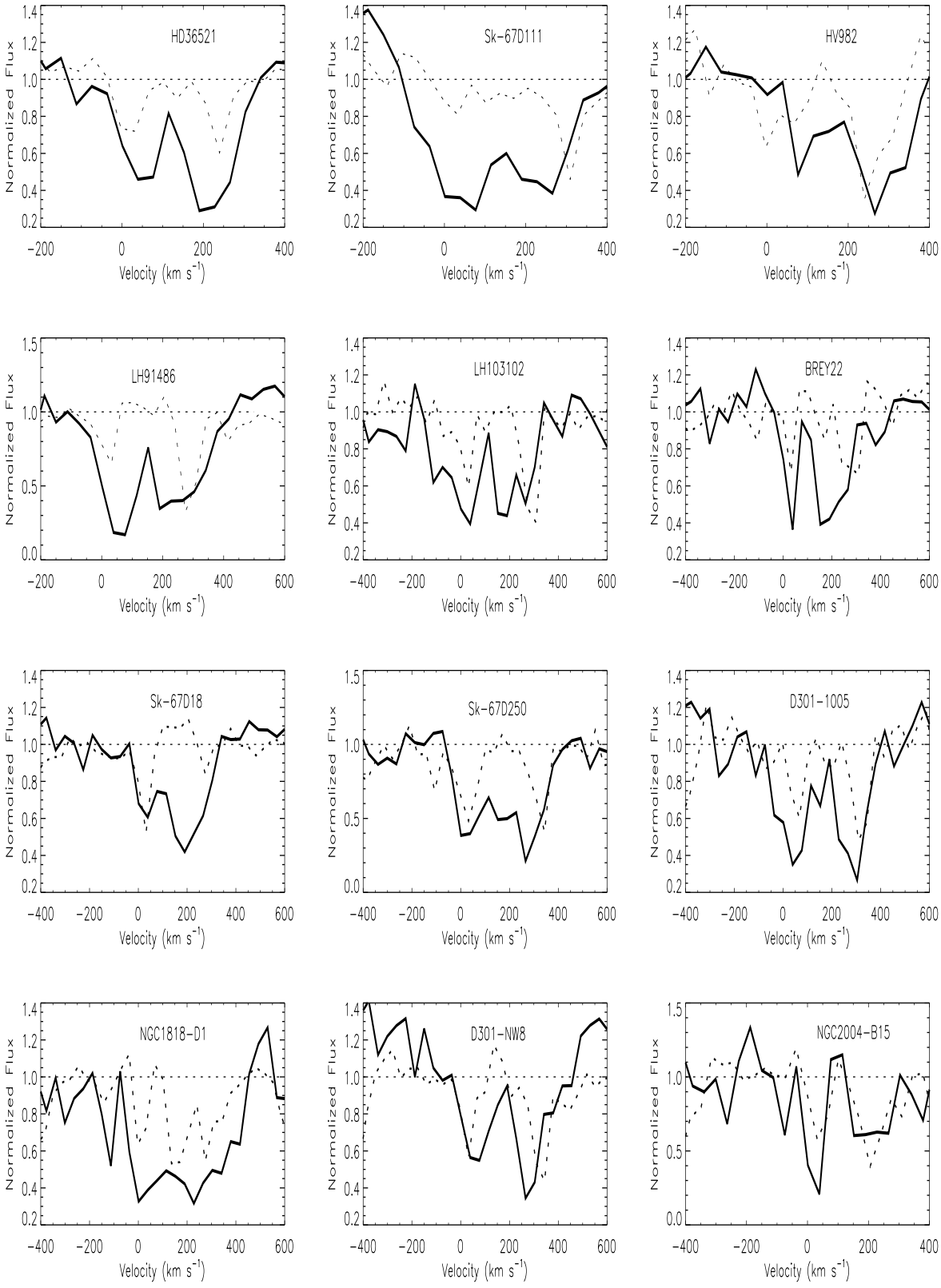


Figure 4.3- *continued*

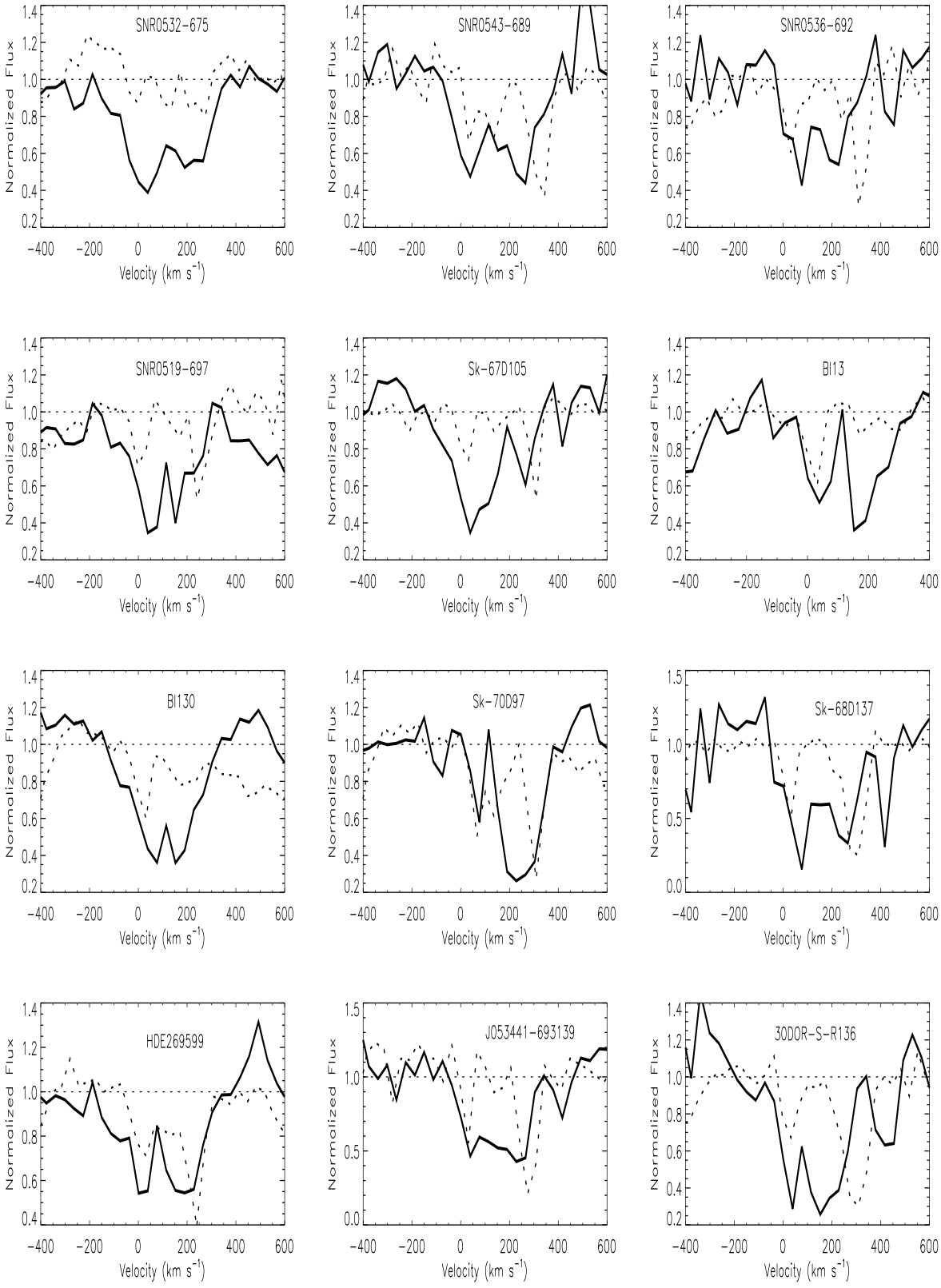


Figure 4.3- *continued*

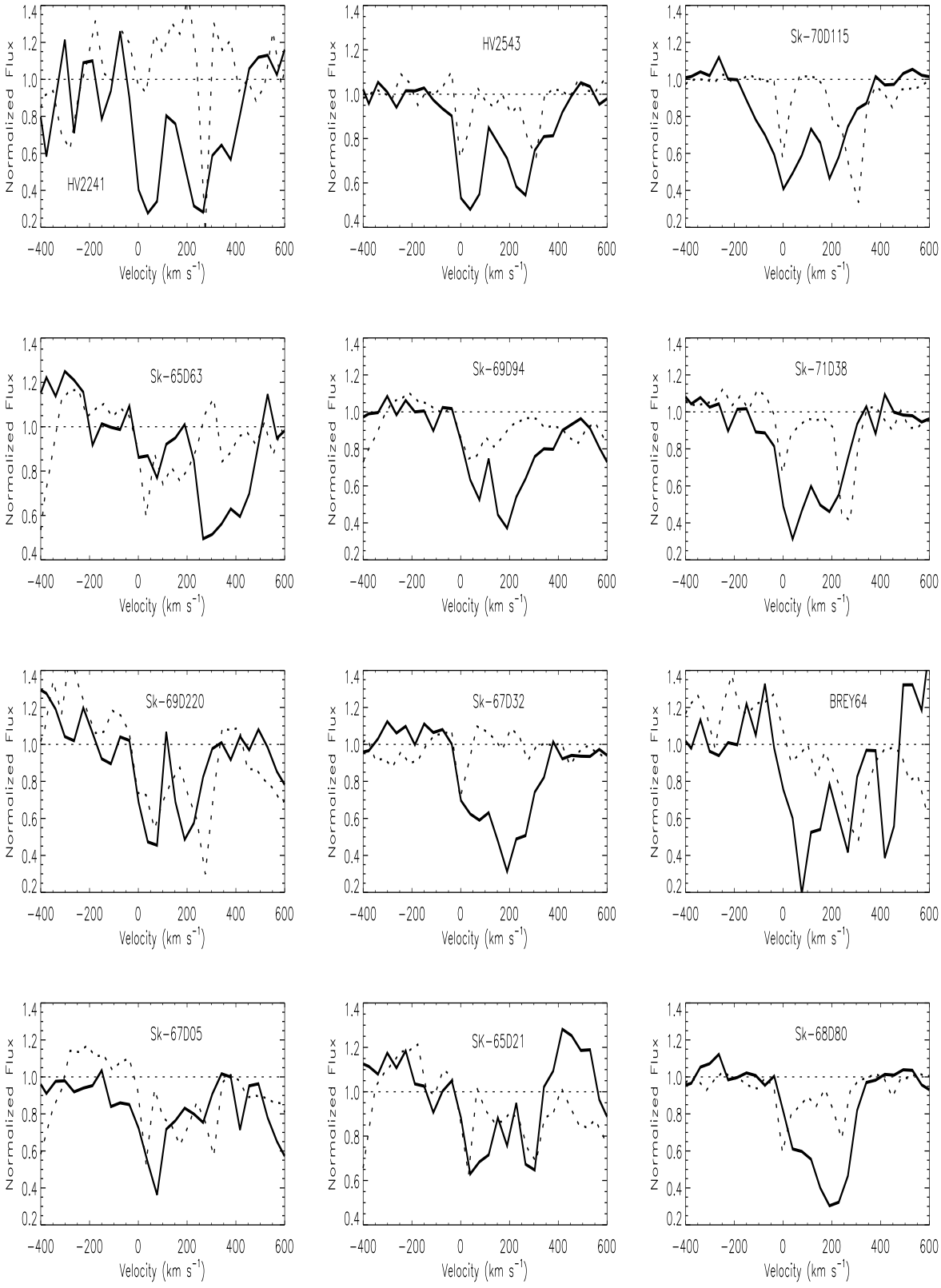


Figure 4.3- *continued*

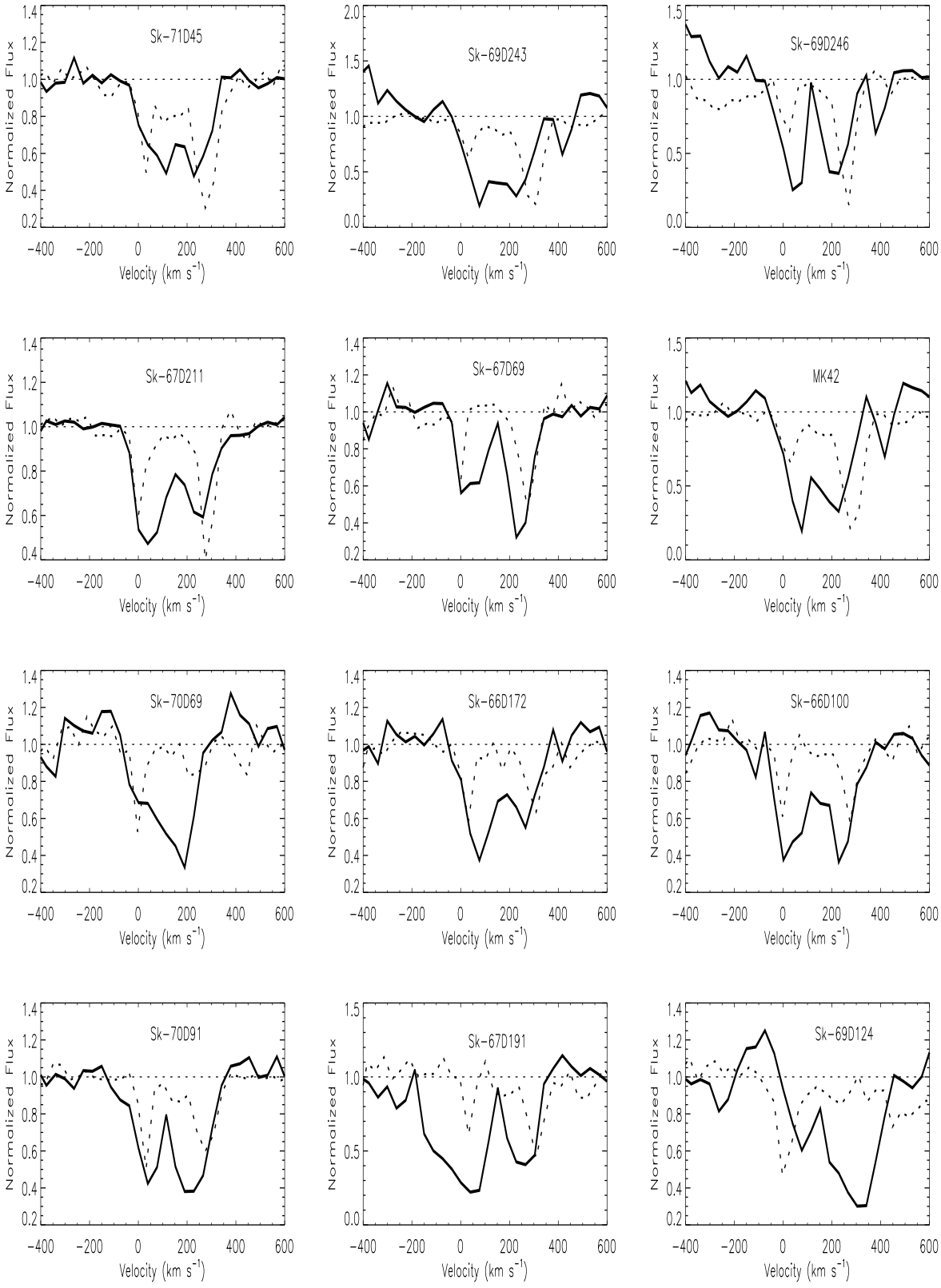


Figure 4.3- *continued*

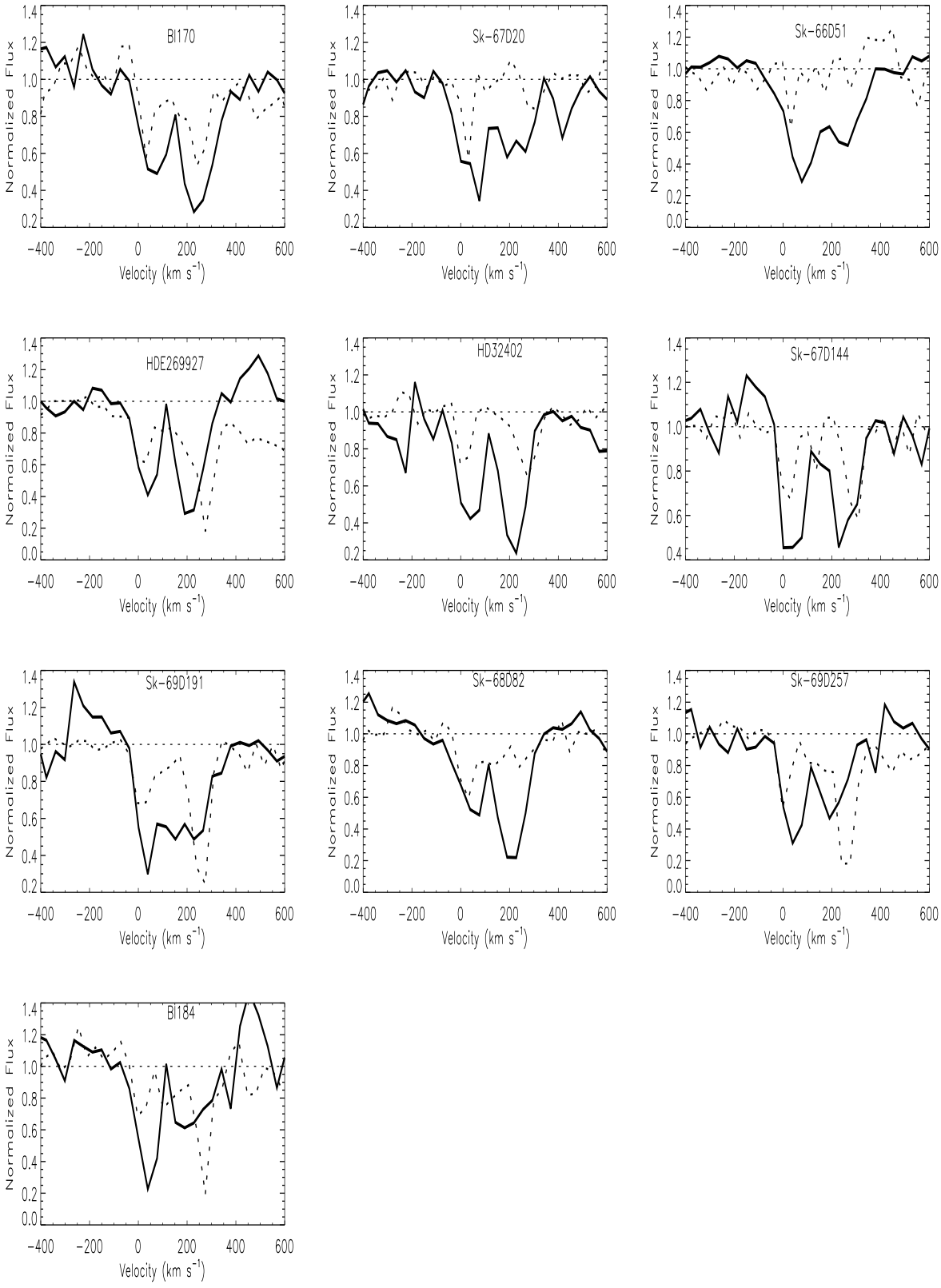


Figure 4.3- *continued*

other broadening mechanisms for the enhanced FWHM values like turbulence, multiple velocity components and collision.

### 4.4.3 Doppler Parameter

The width of an absorption line is a measure of the total velocity distribution in the gas. In the line profile, there may be contribution from thermal motion or other processes like turbulence, bulk flows, broadening of an extended object by the Hubble expansion etc. The line width b, termed as Doppler parameter is defined as b = FWHM/$2\sqrt{2(LN(2))}$.

By measuring the line width, insights into the kinematics of the gas can be studied. The line width, b (km $s^{-1}$) measured using AOD method is free from instrumental blurring as the measurement is based on direct integration of the observed profile. Also *FUSE* is expected to nearly totally resolve the O VI absorption because of it's high resolution which definitely indicates that the observed profile is a true representation of the O VI absorption. Savage et al. found $\langle b \rangle$=61±15km $s^{-1}$ with a median value of 59 km $s^{-1}$ for extragalactic sight lines [343]. Earlier Jenkins [301] found a variation in the value of b from 10.7 to 56 km $s^{-1}$ with median value 27 km $s^{-1}$. Lehner et al. [349] also derived the O VI b-distribution and found a variation from 20 to 60 km $s^{-1}$. O VI velocity dispersions from 33 to 78 km $s^{-1}$ with an average $\langle b \rangle = 45 \pm 11$ km $s^{-1}$ was reported for 22 halo stars [346].

Maximum number of O VI in CIE is found at $2.8\times10^5$ K [150]. At this temperature the thermal Doppler line width should be =17.1 km $s^{-1}$ corresponding to FWHM = 28.5 km $s^{-1}$. The observed line widths for all sight lines of this study ranges from $16.99^{+1.0}_{-1.0}$ km $s^{-1}$ for BREY22 to $80.69^{+4.0}_{-17.0}$ $kms^{-1}$ for SNR0532-675. The median, average and standard deviation of equivalent width are 45.23, 45.32 and 13.29 respectively. The b-values are larger than expected from thermal broadening in gas at $2.8\times10^5$ K. This may be due to different environments dominated by inflow, outflow and turbulent motions. Distribution of the Doppler parameter and the column density is one way to gain information about the temperature and the density of the ISM. For the *FUSE* data a Gaussian profile is found to give a good fit for the distribution of Doppler parameter b. A linear correlation between N(O VI) and b was first discussed by Heckman et al.[350], who studied the trend using extragalactic sight lines and data from early investigations of O VI in the Galaxy. They discussed the correlation between O VI column density and Doppler parameter which is expected in radiatively cooling or conductively heated gas. This correlation extends from the local interstellar medium (LISM) to the Galactic

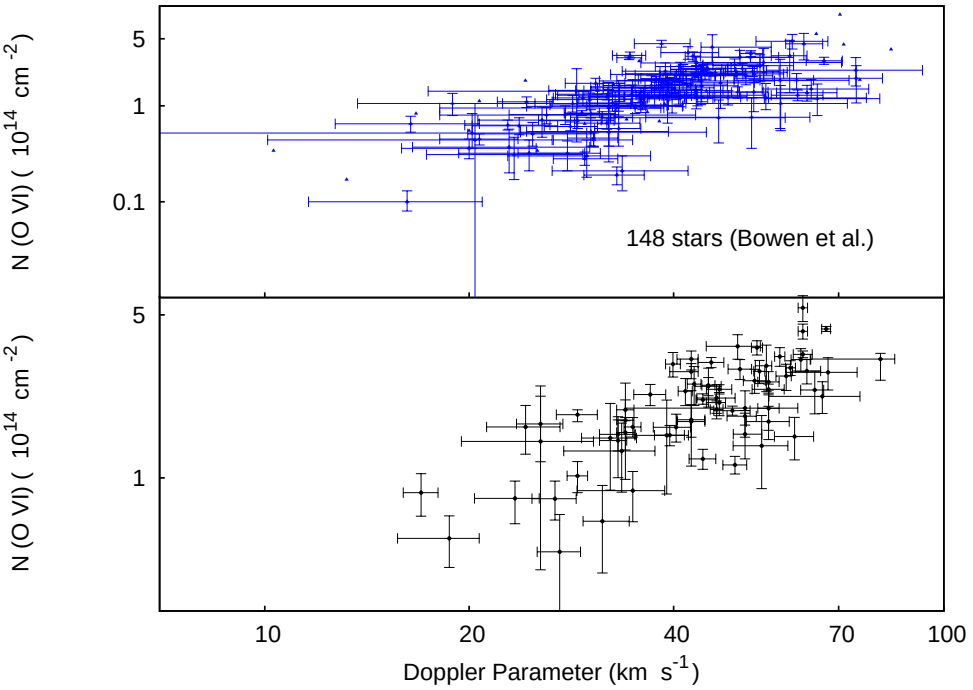


**Figure 4.4:** O VI column density [N(O VI] vs Doppler parameter, b derived for the 70 sight lines (lower panel). The upper panel shows the results obtained by Bowen et al.[319].

disk and halo and beyond [343, 350]. Bowen et al. [319] also found a similar relation in the Galactic disk for O VI. A good correlation between Doppler parameter and O VI column density with Spearman correlation coefficient 0.73 at b >15 km $s^{-1}$ was reported by Lehner et al. [349]. Figure 4.4 presents N(O VI) against Doppler parameter b which gives similar correlation as reported for other studies. For comparison the results of Bowen et al. [319] have also been plotted in the upper panel of Figure 4.4. Heckman et al. [350] suggested that the correlation depends on characteristic velocity which can be explained by the laws of heating or cooling. The correlation suggests a collision dominated ionisation for O VI production [349]. In Figure 4.5, the histogram of the values of b for all sight lines are shown. From Figure 4.5, it is clear that most of the components have b$\gg$b$_{exp}$, where b$_{exp}$ is the b value at temperature where peak O VI abundance is expected. This suggest that nonthermal motions may dominate the broadening mechanism and or multiple unidentified components in the broader profiles [349].

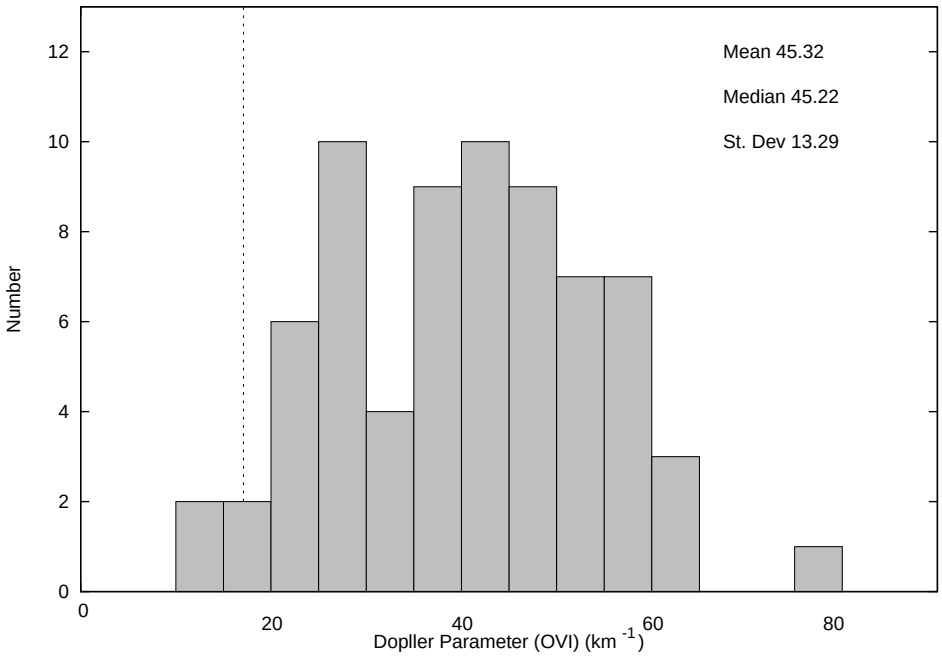


**Figure 4.5:** Doppler parameter distribution of O VI considering a bin size of 5 km $s^{-1}$. The vertical dotted line represents the expected b-value at maximum O VI abundance temperature in CIE.

### 4.4.4 O VI Column Density and Angular Variation

The O VI column densities have been measured using AOD method for all the 70 stars in the LMC [(l,b)=280.5, - 32.9 and d= 50 kpc]. As evident from Table 4.2, there exist significant variations of N(O VI) among the sample. The lowest value of column density has been found to be $4.28\times10^{13}$ atoms $cm^{-2}$ for SK-65D63. For LH91486 the value is highest which is $5.36\times10^{14}$ atoms $cm^{-2}$. This gives a variation of the order of $\sim$ 11 between the two extreme values.

The column density variation with respect to the angular scale may provide us informations on physical properties of the regions in which O VI is produced. Physical dimensions and shapes of the O VI bearing clouds can be understood from the amount of change in N(O VI) and the size scale of variations. Though uniform distribution of hot gas in the Galactic halo was considered [149], soon it became clear that the O VI distribution is not smooth in the Galaxy [343].

**Table 4.4:** Angular scale variations for the 70 targets in the LMC.

| Object Name | RA ($^{hms}$) | Dec ($^\circ\ '\ ''$) | Angular Separation (Degree) | Distance (kpc) | $\mid \triangle$ log N OVI$\mid$ (Dex) |
|---|---|---|---|---|---|
| SK-67D05 | 04 50 18.96 | -67 39 37.9 | 0 | 0 | 0 |
| SK-68D03 | 04 52 15.56 | -68 24 26.9 | 0.77 | 0.54 | $13.80^{+1.31}_{-0.73}$ |
| BI13 | 04 53 06.48 | -68 03 23.1 | 0.48 | 0.33 | $12.79^{+1.00}_{-0.63}$ |
| SK-67D18 | 04 55 14.90 | -67 11 24.5 | 0.67 | 0.47 | $13.73^{+0.57}_{-0.39}$ |
| Sk-67D20 | 04 55 31.50 | -67 30 01.0 | 0.52 | 0.36 | $13.48^{+1.00}_{-0.63}$ |
| PGMW-3070 | 04 56 43.25 | -66 25 02.0 | 1.39 | 0.97 | $13.13^{+0.57}_{-0.39}$ |
| LH103102 | 04 56 45.40 | -66 24 45.9 | 1.40 | 0.98 | $13.75^{+0.00}_{-0.87}$ |
| LH91486 | 04 56 55.58 | -66 28 58.0 | 1.34 | 0.94 | $14.55^{+1.13}_{-0.68}$ |
| PGMW-3223 | 04 57 00.80 | -66 24 25.3 | 1.41 | 0.99 | $13.91^{+1.00}_{-0.63}$ |
| HV2241 | 04 57 15.83 | -66 33 54.8 | 1.29 | 0.90 | $14.26^{+1.13}_{-0.68}$ |
| HD32402 | 04 57 24.19 | -68 23 57.2 | 0.99 | 0.69 | $13.82^{+0.89}_{-0.58}$ |
| SK-67D32 | 04 59 52.30 | -67 56 55.0 | 0.95 | 0.66 | $13.60^{+1.00}_{-0.63}$ |
| SK-65D21 | 05 01 22.33 | -65 41 48.1 | 2.25 | 1.57 | $14.01^{+0.81}_{-0.54}$ |
| HV2274 | 05 02 40.96 | -68 24 21.3 | 1.38 | 0.96 | $13.47^{+0.74}_{-0.50}$ |
| Sk-66D51 | 05 03 10.20 | -66 40 54.0 | 1.58 | 1.11 | $14.19^{+1.62}_{-0.95}$ |
| NGC1818-D1 | 05 04 32.56 | -66 24 51.0 | 1.86 | 1.30 | $14.01^{+1.61}_{-0.80}$ |
| SK-70D69 | 05 05 18.73 | -70 25 49.8 | 3.08 | 2.15 | $13.67^{+0.33}_{-0.22}$ |
| Sk-67D69 | 05 14 20.16 | -67 08 03.5 | 2.37 | 1.65 | $13.52^{+0.81}_{-0.54}$ |
| MACHO78-6097 | 05 18 04.70 | -69 48 19.0 | 3.30 | 2.31 | $13.42^{+1.31}_{-0.73}$ |
| BI130 | 05 18 06.06 | -69 14 34.5 | 3.00 | 2.09 | $14.14^{+1.13}_{-0.68}$ |
| SK-69D94 | 05 18 14.53 | -69 15 01.0 | 3.01 | 2.10 | $13.28^{+1.00}_{-0.63}$ |
| SNR0519-697 | 05 18 44.20 | -69 39 12.4 | 3.26 | 2.28 | $13.95^{+0.62}_{-0.42}$ |
| BREY22 | 05 19 16.40 | -69 39 19.5 | 3.30 | 2.30 | $13.99^{+0.81}_{-0.54}$ |
| HD269445 | 05 22 59.87 | -68 01 46.6 | 3.10 | 2.16 | $14.11^{+0.00}_{-0.87}$ |
| SK-69D124 | 05 25 18.37 | -69 03 11.1 | 3.51 | 2.45 | $13.98^{+0.81}_{-0.54}$ |
| SK-67D105 | 05 26 06.37 | -67 10 57.6 | 3.47 | 2.42 | $13.89^{+1.13}_{-0.68}$ |
| SK-67D106 | 05 26 15.20 | -67 29 58.3 | 3.43 | 2.39 | $14.07^{+0.44}_{-0.33}$ |
| SK-67D107 | 05 26 20.67 | -67 29 55.4 | 3.44 | 2.40 | $14.38^{+1.61}_{-0.80}$ |
| HD36521 | 05 26 30.32 | -68 50 25.4 | 3.55 | 2.48 | $12.97^{+0.52}_{-0.36}$ |
| SK-68D80 | 05 26 30.43 | -68 50 26.6 | 3.55 | 2.48 | $13.80^{+1.31}_{-0.73}$ |
| SK-68D82 | 05 26 45.31 | -68 49 52.8 | 3.57 | 2.49 | $13.17^{+0.81}_{-0.54}$ |
| BI170 | 05 26 47.79 | -69 06 11.7 | 3.65 | 2.55 | $13.75^{+0.00}_{-0.87}$ |
| SK-67D111 | 05 26 47.95 | -67 29 29.9 | 3.48 | 2.43 | $14.01^{+1.13}_{-0.68}$ |
| HV2543 | 05 27 27.40 | -67 11 55.4 | 3.59 | 2.51 | $13.19^{+0.89}_{-0.58}$ |
| SK-70D91 | 05 27 33.74 | -70 36 48.3 | 4.43 | 3.09 | $13.80^{+1.31}_{-0.73}$ |
| Sk-66D100 | 05 27 45.59 | -66 55 15.0 | 3.69 | 2.57 | $14.02^{+1.13}_{-0.68}$ |
| HDE269599 | 05 28 22.68 | -69 08 32.2 | 3.80 | 2.65 | $13.50^{+1.31}_{-0.73}$ |
| SK-65D63 | 05 28 39.50 | -65 39 01.1 | 4.29 | 3.00 | $14.13^{+0.40}_{-0.37}$ |
| HV982 | 05 29 52.50 | -69 09 22.0 | 3.93 | 2.74 | $14.01^{+0.89}_{-0.58}$ |
| SK-70D97 | 05 30 11.35 | -70 51 42.2 | 4.75 | 3.32 | $14.11^{+0.67}_{-0.46}$ |
| Sk-67D144 | 05 30 12.22 | -67 26 08.4 | 3.81 | 2.66 | $13.43^{+1.00}_{-0.63}$ |

Continued on Next Page...

Table 4.4 – Continued

| Object Name | RA ($^{hms}$) | Dec ($^\circ\ '\ ''$) | Angular Separation (Degree) | Distance (kpc) | $\mid \triangle$ log N OVI$\mid$ (Dex) |
|---|---|---|---|---|---|
| BI184 | 05 30 30.60 | -71 02 31.3 | 4.89 | 3.41 | $14.14^{+1.61}_{-0.80}$ |
| NGC2004-B15 | 05 30 36.58 | -67 17 42.3 | 3.87 | 2.70 | $13.26^{+0.74}_{-0.50}$ |
| SK-71D38 | 05 30 38.77 | -71 01 47.9 | 4.89 | 3.41 | $14.17^{+1.31}_{-0.73}$ |
| Sk-71D45 | 05 31 15.55 | -71 04 08.9 | 4.95 | 3.46 | $13.73^{+0.81}_{-0.54}$ |
| SK-67D166 | 05 31 44.31 | -67 38 00.6 | 3.93 | 2.75 | $13.10^{+1.31}_{-0.73}$ |
| SK-67D168 | 05 31 52.10 | -67 34 20.8 | 3.95 | 2.76 | $12.46^{+0.00}_{-0.87}$ |
| SNR0532-675 | 05 32 23.00 | -67 31 02.0 | 4.01 | 2.80 | $14.14^{+1.13}_{-0.68}$ |
| SK-67D191 | 05 33 34.12 | -67 30 19.6 | 4.12 | 2.88 | $14.40^{+1.62}_{-0.95}$ |
| HV5936 | 05 33 39.00 | -66 37 39.8 | 4.33 | 3.02 | $13.87^{+1.31}_{-0.73}$ |
| Sk-69D191 | 05 34 19.39 | -69 45 10.0 | 4.50 | 3.14 | $13.26^{+1.31}_{-0.73}$ |
| J053441-693139 | 05 34 41.30 | -69 31 39.0 | 4.45 | 3.11 | $13.50^{+0.44}_{-0.30}$ |
| Sk-67D211 | 05 35 13.92 | -67 33 27.0 | 4.27 | 2.98 | $14.00^{+1.00}_{-0.63}$ |
| BREY64 | 05 35 54.45 | -68 59 07.4 | 4.41 | 3.08 | $12.85^{+0.40}_{-0.27}$ |
| SNR0536-692 | 05 36 07.70 | -69 11 52.6 | 4.47 | 3.12 | $13.61^{+0.89}_{-0.58}$ |
| SK-69D220 | 05 36 43.83 | -69 29 47.4 | 4.61 | 3.22 | $13.51^{+1.61}_{-0.80}$ |
| Sk-66D172 | 05 37 05.56 | -66 21 35.7 | 4.74 | 3.31 | $14.05^{+1.61}_{-0.80}$ |
| BI253 | 05 37 34.49 | -69 01 09.8 | 4.56 | 3.18 | $13.64^{+1.31}_{-0.73}$ |
| SK-68D137 | 05 38 24.77 | -68 52 32.8 | 4.61 | 3.22 | $13.71^{+1.13}_{-0.68}$ |
| MK42 | 05 38 42.10 | -69 05 54.7 | 4.67 | 3.26 | $14.07^{+0.74}_{-0.50}$ |
| SK-69D243 | 05 38 42.57 | -69 06 03.2 | 4.68 | 3.26 | $13.84^{+0.81}_{-0.54}$ |
| 30DOR-S-R136 | 05 38 51.70 | -69 06 00.0 | 4.69 | 3.27 | $13.59^{+0.67}_{-0.46}$ |
| SK-69D246 | 05 38 53.50 | -69 02 00.7 | 4.68 | 3.26 | $14.25^{+1.61}_{-0.80}$ |
| HDE269927 | 05 38 58.25 | -69 29 19.1 | 4.79 | 3.35 | $13.57^{+1.00}_{-0.63}$ |
| SK-69D257 | 05 39 58.91 | -69 44 03.2 | 4.95 | 3.46 | $14.09^{+1.13}_{-0.68}$ |
| SNR0543-689 | 05 43 07.20 | -68 58 52.0 | 5.04 | 3.52 | $12.98^{+0.74}_{-0.50}$ |
| D301-1005 | 05 43 08.30 | -67 50 52.4 | 4.99 | 3.49 | $14.04^{+1.31}_{-0.73}$ |
| SK-67D250 | 05 43 15.48 | -67 51 09.6 | 5.00 | 3.49 | $13.08^{+1.31}_{-0.73}$ |
| D301-NW8 | 05 43 15.96 | -67 49 51.0 | 5.01 | 3.49 | $13.02^{+0.00}_{-0.87}$ |
| SK-70D115 | 05 48 49.76 | -70 03 57.5 | 5.78 | 4.03 | $13.55^{+0.81}_{-0.54}$ |

Notes. All the distances have been calculated from SK-67D05 assuming the distance of the absorbing cloud to be 40 kpc from the Sun.

Howk et al. [306] found large variations in O VI column densities over small angular scales towards 12 LMC and 11 SMC stars. They found column density variations for the smallest scales with a value of $\triangle\theta \sim 1.8$. No significant N(O VI) variation was found towards 4 stars in NGC 6752 that are separated by 2.2 – 8.9 [351]. The sight lines in this study are separated by angular distances of $0.024 \leq \triangle\theta \leq 5.779$. Column 4 and 5 of Table 4.4 give the angular separation and distance of each source from the Sk-67D05 (first source) respectively. The distances have been calculated assuming O VI absorption by HVCs located in the halo of the galaxy towards the LMC at a distance of 40 kpc

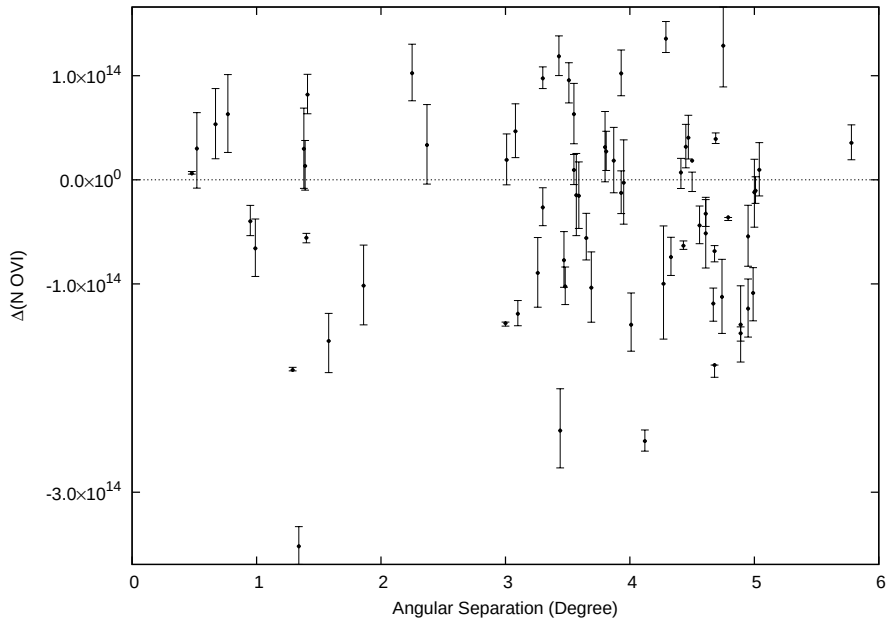


**Figure 4.6:** O VI column density [log(O VI] vs angular separation for the 70 sight lines.

from the Sun. The logarithmic difference in column densities between the first source and others for total velocity is calculated which is presented in column 6 of Table 4.4.

As can be seen from Table 4.4 there exist clear variation in the amount of N(O VI) over all angular scales. In some earlier works (e.g. [351], [306] etc.) small scale variations of N(O VI) have been reported. But we found much smaller variation of it. We found variation from a minimum of 0.28 pc to 4.03 kpc. The smallest scale for which O VI column density variations has been found is $\triangle\theta \sim 1.44$ ($\sim 0.28$ pc) for the closest pairing stars HD36521 and SK-68D80 whereas the widest pairing stars differ by 5.78 (4.03 kpc). Figure 4.6 shows the difference in column densities integrated over the total velocity range against angular scale. This figure suggest significant O VI variation over small angular scales. This result definitely confirms the patchiness of O VI in the Galaxy.

Howk et al.[306] discuss the angular correlation function of the O VI measurements, finding no preferred angular scale for the O VI variations. Savage et al. [343] showed that the variations seen toward the LMC and SMC extend to larger angular scales. They favored models in which the O VI-bearing medium is composed of small complex cloud-like or sheet-like distributions of material [306, 343].

### 4.4.5 Scale height

One of the aim of this work is to study the distribution of O VI in the Galactic plane. Though these has been reported earlier [302, 319, 343, 347], as the numbers of sight lines in this study is large, it may be worthwhile to revisit the O VI distribution. An exponential gas distribution with n($|z|$)=$n_0$ exp (-$|z|$/h) where h is scale height is assumed. The column density N(x) perpendicular to the plane for an object with latitude b can be given by N(x) sin $|b|$=$n_0$h[1-exp (-$|z|$/h)], where N(x) sin $|b|$ is the line-of-sight column density of an objects. For extra-galactic objects ($|z| \gg$ h), N(x) sin $|b|$=$n_0$h.

The midplane density $n_0$ has been estimated to be $2.8\times10^{-8}$ cm$^{-3}$ [302] and using *Copernicus* data O VI scale height found to be 0.3 kpc. The *Copernicus* O VI observations have been reanalyzed by Shelton & Cox [352] and they found that the midplane O VI density beyond the Local Bubble is $(1.3 - 1.5)\times10^{-8}$ cm$^{-3}$ for an O VI absorbing layer with h$\sim$ 3 kpc. Savage et al. [307] estimating $n_0 = 2.0\times10^{-8}$ cm$^{-8}$ from *Copernicus* O VI survey derived scale height h>2 kpc. Using *FUSE* data of 100 extragalactic objects Savage et al.[343] derived a scale height of h$\sim$2.5 kpc.

The scale height for all the 70 sight lines have been measured here. For a midplane density $n_0$=$1.64\times10^{-8}$ cm$^{-3}$ [347], scale height has been measured using the simple relation h=N(x) sin $|b|/n_0$. The value ranges from 2.73 to 2.95 kpc. The average values of the O VI scale height is 2.85$\pm$0.7 kpc. Savage & Wakker [347] derived the O VI scale height to be 2.6$\pm$0.5 kpc. Scale height have also been calculated for all the sight lines for the column density derived in the range from minimum to 100 kms$^{-1}$. The average scale height in this case has been found to be 2.80 kpc.

The error estimation in deriving the O VI scale height was first addressed by Savage et al. [353]. The exponential decrease with height nature of O VI above the Galactic plane is not smooth and planar but patchy. So a logarithmic patchiness parameter $\sigma_p$ is introduced to the $\chi^2$ minimization process such that $\sigma=(\sigma_c^2 + \sigma_z^2 + \sigma_p^2)^{1/2}$ where $\sigma_c$ is the logarithmic column density error and $\sigma_z$ is the logarithmic distance error. For extragalactic sight lines the error in distance does not influence the fit [347] so this error has been ignored. In order to obtain reduced $\chi^2$ =1.0, $\sigma_p$ is kept as free parameter. The 1 $\sigma$ error in the scale height is determined by estimating the the value of h where $\chi^2$ =$\chi^2$(min) +2.3 contour in h-log($n_0$h) space.

From the O VI scale height value, the temperature of the ionized plasma can be found out as derived by Savage & Wakker [347]. Considering hydrostatic equilibrium at temperature T for an isothermal gas, the scale height is given by h=kT/$\langle m \rangle g(|z|)$.

The value of gravitational acceleration toward the disk g($|z|$), in the solar neighbourhood for a distance 1-10 kpc is $\sim 10^{-8}$cm s$^{-2}$ [354]. Considering average mass per particle $\langle m \rangle$=0.73m$_H$, for a scale height h=2.85 kpc the temperature of the gas is found to be T$\sim$ 3.84$\times$ $10^5$ K. This temperature is $\sim$ 1.3 times larger than the transition temperature of O VI. Savage & Wakker [347] derived the required temperature as $\sim$ 0.8$\times$ $10^6$ K for scale height value h=3 kpc.

## 4.5 Summary and Conclusion

The properties of O VI in the MW along the lines of sight to 70 stars in the LMC have been studied using *FUSE* spectra. The observed absorption lines are studied using AOD method which reveal significant variation in O VI column densities over small angular scale. The main conclusions of this work are as follows:

• For all 70 sight lines, strong O VI absorptions at 1031.926 Å in the MW is found. The highest column density measured for the MW is log N(OVI) = 14.73 atoms cm $^{-2}$ and the minimum value is log N(OVI) = 13.68 atoms cm $^{-2}$. The mean MW O VI column density is found to be 14.29 atoms cm$^{-2}$. The median value of our sample is 14.21 atoms cm$^{-2}$. The logarithm of the column densities perpendicular to the Galactic plane varies between 13.42 and 14.50 with average values of 14.03 atoms cm$^{-2}$.

• There is a significant variations of O VI column densities on all scales studied by this observation (0.024 - 5.779). The smallest scale for which O VI column density variation has been found is $\sim$ 1.44 ($\sim$ 0.28 pc).

• The measured O VI column densities can be described by a patchy exponential distribution in the MW which is in accordance with earlier measurements of O VI absorption for the Galaxy.

• The velocity dispersions (b-values) of the O VI absorption profiles ranges from 16.99 to 80.69 km s$^{-1}$. The median, average and standard deviation of equivalent width are 45.23, 45.32 and 13.29 respectively. The b-values are larger than expected from thermal broadening in gas at 2.8$\times$10$^5$ K. This may be due to different environments dominated by inflow, outflow and turbulent motions.

• The broad ($\geq$16.99 km s$^{-1}$) O VI absorption profiles suggest collisional ionization at the interface of warm-hot ISM be the mechanism that produces this ion.

• O VI column density and the Doppler parameter, b, are found to be correlated for the considered sample of sight lines. This confirms earlier results.

• Kinematical comparisons of Fe II and O VI line profiles reveal the presence of HVC and/or IVC components in the O VI absorption along all sight lines. But in Fe II profiles either of these components have not been observed. The distribution of O VI is significantly different than that of Fe II. The broad absorption profiles of O VI traces more extended layers than that of the Fe II-bearing layer.

• For a midplane density $n_0$=1.64×$10^{-8}$ $cm^{-3}$, the O VI scale height is found to be 2.85±0.7 kpc. This is in accordance with earlier results.

⋆⋆⋆